A EUROPEAN JOURNAL OF CHEMICAL BIOLOGY

CHEMBIOCHEM

SYNTHETIC BIOLOGY & BIO-NANOTECHNOLOGY

Accepted Article

Title: Glycosylated Cell Penetrating Peptides, GCPPs

Authors: Ivan Gallego, Alicia Rioboo, Jose J Reina, Bernardo Díaz, Ángeles Canales, F Javier Cañada, Jorge Guerra-Varela, Laura Sánchez, and Javier Montenegro

To be cited as: *ChemBioChem* 10.1002/cbic.201800720

Link to VoR: http://dx.doi.org/10.1002/cbic.201800720

A Journal of

WILEY-VCH

www.chembiochem.org

Glycosylated Cell Penetrating Peptides, GCPPs

Iván Gallego,[a] Alicia Rioboo,[a] Dr. José J. Reina,[a] Bernardo Díaz,[b,c] Dr. Ángeles Canales,[c] Dr. F. Javier Cañada,[b] Dr. Jorge Guerra-Varela,[d] Prof. Laura Sánchez,[d] Dr. Javier Montenegro*[a]

Abstract: The cell membrane regulates the exchange of molecules and information with the external environment. However, this control barrier hinders the delivery of exogenous bioactive molecules that can be applied to correct cellular malfunctions. Therefore, the traffic of macromolecules across the cell membrane represents a great challenge for the development of the next generation of therapies and diagnostic methods. Cell penetrating peptides are short peptide sequences capable of delivering a broad range of biomacromolecules across the cellular membrane. However, penetrating peptides still suffer from limitations mainly related with their lack of specificity and potential toxicity. Glycosylation has emerged as a potential promising strategy for the biological improvement of synthetic materials. In this work we have developed a new convergent strategy for the synthesis of penetrating peptides functionalized with glycan residues by an oxime bond connection. We have systematically characterized the uptake efficiency and the intracellular distribution of these glycopeptides by flow cytometry, confocal microscopy and in zebrafish animal models. The incorporation of these glycan residues into the peptide structure influenced the internalization efficiency and the cellular toxicity of the resulting glycopeptide hybrids in the different cell lines tested. The results reported here highlight the potential of the glycosylation of penetrating peptides to modulate their activity.

Introduction

The plasma membrane of eukaryotic cells is a control barrier with selective permeability that separates the cell from the external environment.[1,2] However, this barrier and the related cell associated transport mechanisms such as endocytosis, prevent the cytosolic delivery of exogenous hydrophilic molecules with high molecular weight. As a consequence, the search of new biocompatible molecular transporters[3] has been intensified in the last two decades.[3–5] More than twenty years ago it was accidently discovered that certain protein domains, enriched in cationic amino acids, were responsible for promoting the translocation of some proteins through the plasma membrane of cells.[4] The findings of Green, Loewehstein, Frankel and Pabo documented the efficient internalization of the trans-activator of transcription of the TAT protein of the human immunodeficiency virus (HIV-1) when added to the cell culture medium.[6,7] In 1997 B. Lebleu reported that the peptide function with penetrating properties belonged to the cationic domain that was called the TAT peptide (TAT_{49-57}, RKKRRQRRR).[8] These membrane translocation properties were also found in the Antennapedia homeodomain discovered for the first time in *Drosophila* by Prochiantz in 1994.[9] These penetrating peptide sequences were generally short and enriched in basic amino acids such as lysine and arginine and they were denominated as cell penetrating peptides (CPPs).[4]

Naomi Sakai and Stefan Matile in Geneva University studied and demonstrated that CPPs were able to translocate the membrane by a counterion exchange mechanism.[10,11] In the arginine amino acids, the guanidinium group with a pKa of around 12, cannot be deprotonated at physiological pH. Therefore, counterion scavenging is the only way to minimize electrostatic repulsion in oligo or polyguanidiniums.[10,12,13] This exchange of negative counterions allows CPPs to acquire amphiphilc character with both hydrophilic and hydrophobic properties, which triggers their membrane translocation.[10,11] As cellular membranes are enriched in anionic counterions (i.e. glycosaminoglycans, anionic lipids), CPPs use these amphiphilic anions to anchor to the cells surface and translocate the lipid bilayer.

The group of Paul Wender in Stanford systematically studied the TAT_{49-57} peptide sequence and artificial analogues, demonstrating that between eight to ten cationic amino acids were optimal.[14] These studies also showed that oligolysines were less effective than the oligoarginines analogues[15] and triggered the development of synthetic penetrating oligoarginines.[14,16] Similar uptake properties were found for the enantiomeric TAT_{49-57} peptide and in penetrating peptoids with the guanidinium side chains anchored at the nitrogen of the amide group.[15] All these findings and subsequent studies have allowed the extension of these properties to a broad range of natural and artificial scaffolds with new and improved penetrating capabilities as well as new methods for internalization characterization.[17–25] Interesting penetrating properties were further discovered in different natural and artificial structures such as polyprolines,[26] guanidinyl glycosides,[27,28] β-peptides,[29] nucleic acids (PNAs),[30] non-peptidic guanidinylated dendritic structures,[31] self-assembled nanofibres,[32,33] synthetic polymers,[34–37] supramolecular structures[38–40] and polydisulfides.[41–44]

[a] Centro Singular de Investigación en Química Biolóxica e Materiais Moleculares (CIQUS), Departamento de Química Orgánica, Universidade de Santiago de Compostela, Campus Vida, 15782 Santiago de Compostela, Spain.
E-mail: : javier.montenegro@usc.es
[b] Centro de Investigaciones Biológicas (CIB) del CSIC, C/Ramiro de Maetzu 9, CP 28040, Madrid.
[c] Departamento de Biología Estructural y Química, Fac. Ciencias Químicas Univ. Complutense de Madrid, Avd/ Complutense s/n, CP. 28040, Madrid.
[d] Departamento de Zooloxía, Xenética e Antropoloxía Física. Facultade de Veterinaria Universidade de Santiago de Compostela, 27002, Lugo, Spain.

Supporting information for this article is given via a link at the end of the document.((Please delete this text if not appropriate))

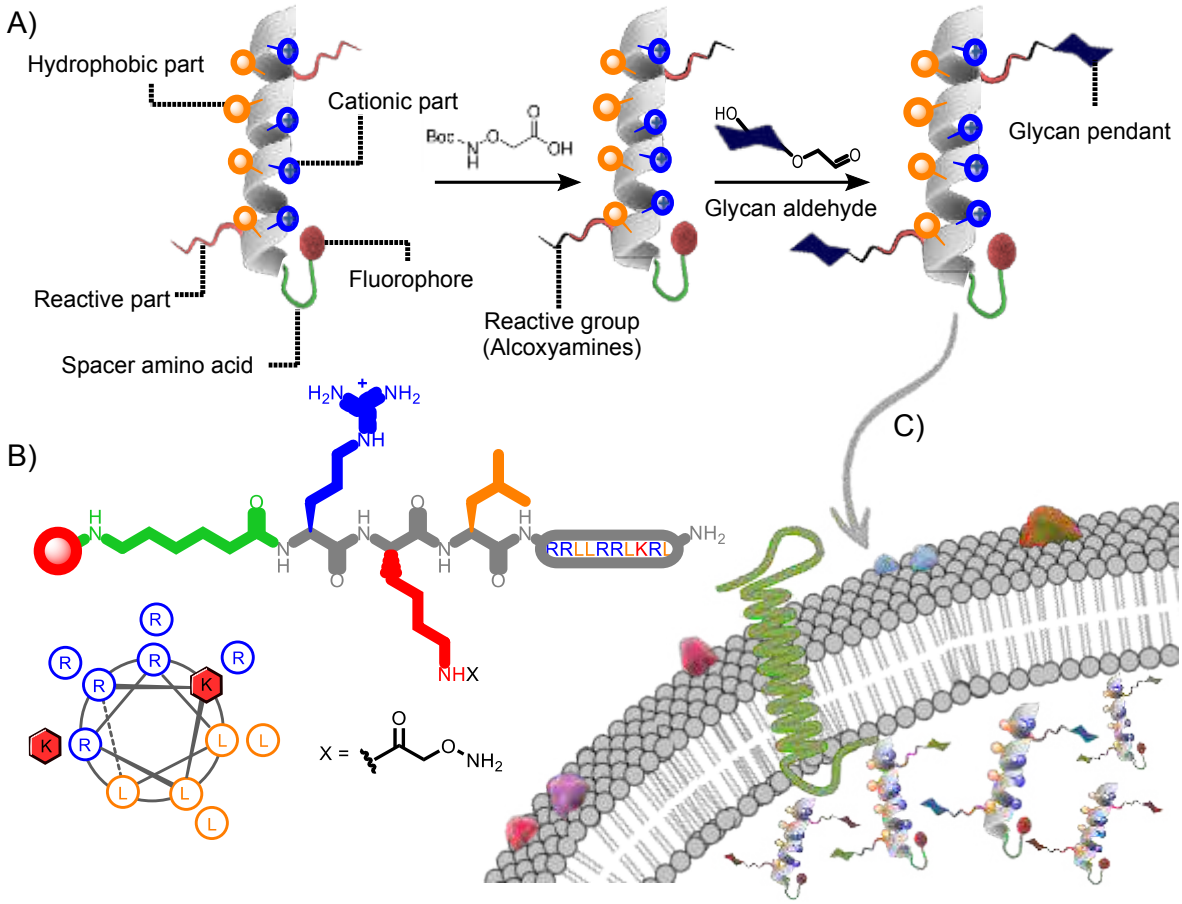

Figure 1. Peptide structure and membrane transport. A) The peptide segregated domains along an alpha helical scaffold. The reactive groups (alkoxyamines) point to opposite directions at the interphase of the hydrophilic and hydrophobic domains. The primary peptide structure is equipped with reactive alkoxyamines to anchor different glycan aldehydes. The final glycopeptide hybrids contain a fluorescent probe (red dot) anchored to the N-terminal region of the peptide to monitor and quantify their cellular internalization. B) Linear peptide primary sequence and heptad-based wheel diagram for the helical conformation of the peptide. C) Membrane translocation and cellular internalization is modulated by the glycan residue.

After these structural and functional discoveries, the potential of the CPPs has led to the development of myriad of penetrating peptide sequences for the cellular internalization of different payloads.[45–49] These strategies have deliver excellent peptides and related analogues with applications in gene delivery, liposomes functionalization, nanoparticles decoration and therapeutic proteins delivery.[4,37,57,58,48,50–56] However, despite all the advances in the field, cell penetrating peptides still have some limitations mainly related to their selectivity and toxicity.[59–62] For instance, the cationic character of CPPs, which is required for membrane anchoring and translocation, constitutes an important drawback, as highly cationic molecules tend to stick non-specifically in living tissues.[59–62] The potential modification of these peptides with targeting or biocompatible functionalities emerges as a promising strategy to improve the selectivity and minimize toxicity of CPPs.[61,63]

Glycan conjugation has been extensively applied for the targeted delivery of different biomolecular scaffolds, including polymers, nanoparticles and nucleic acids.[43,64–71] This strategy is aimed to target cellular membrane receptors and accumulate the glycan-tagged ensembles at a particular tissue.[72,73] Natural *N*-linked glycan scaffolds can be used as an alternative to antibodies for targeted delivery to cells expressing the CD22 receptor.[74] Certain glycans, which are found exclusively on pathogenic bacteria, could also be exploited for therapeutic targeting and diagnosis.[75,76] Nanomaterials and supramolecular structures bearing glycans can also find applications in biomedicine, vaccines, bacterial infections, cancer treatments, nuclear magnetic resonance imaging, etc.[77–79] Glycan-coated quantum dots have been delivered in HeLa and SV40 epithelial cells.[80] Liposomes decorated with glycan ligands for CD169/Sn recognition were developed for macrophages targeted delivery.[81] Multivalent glycopeptide dendrimers were also applied in cancer immunotherapy, autoimmunity and infectious diseases.[82] Additionally, multivalent systems like globular

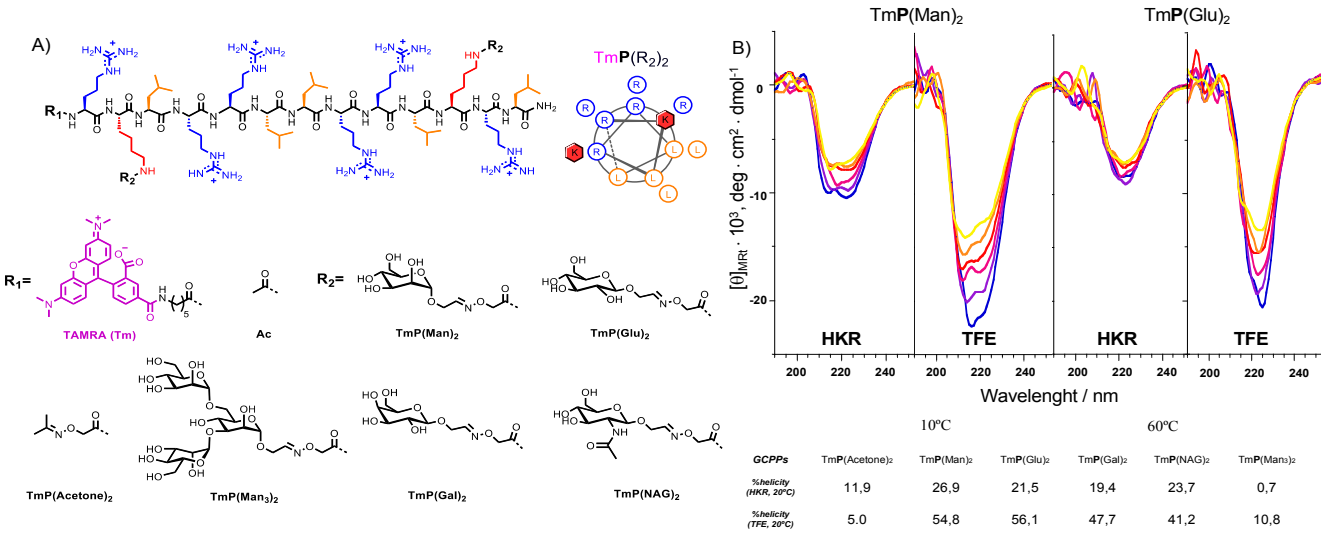

	10ºC			60ºC		
GCPPs	TmP(Acetone)2	TmP(Man)2	TmP(Glu)2	TmP(Gal)2	TmP(NAG)2	TmP(Man3)2
%helicity (HKR, 20ºC)	11,9	26,9	21,5	19,4	23,7	0,7
%helicity (TFE, 20ºC)	5.0	54,8	56,1	47,7	41,2	10,8

Figure 2. Peptide structure and circular dichroism spectra. A) Linear peptide structure with the amino acid side chains in different colors: cationic (Arg) in blue, hydrophobic (Leu) in orange and modified lysine residues (Lys-R_2) in red. Substituent in the N-terminal $\mathbf{R_1}$: TAMRA fluorophore (Tm), **Ac**: Acetyl. Substituents in the modified lysines $\mathbf{R_2}$: acetone and the oximes derivatives of: α-D-Mannose Tm**P**(Man)$_2$, β-D-Glucose Tm**P**(Glu)$_2$, β-D-Galactose Tm**P**(Gal)$_2$, N-acetyl-β-D-glucosamine Tm**P**(NAG)$_2$, and Mannose tri-saccharide Tm**P**(Man$_3$)$_2$. B) CD spectra of Tm**P**(Man)$_2$ and Tm**P**(Glu)$_2$ in different conditions TFE (trifluoroethanol) and HKR buffer (pH 7.4).

glycofullerenes enhance molecular recognition towards specific lectins.[83,84]

Carbohydrate ligands can bind different targets and membrane-bound receptors such as lectins, which can trigger endocytic processes.[72,85] Mono/oligosaccharides like mannose derivatives exhibit strong binding to the C-type lectin DC-SIGN on the surface of dendritic cells,[86] C-type lectin receptors on macrophages[87] and the plant lectin concanavalin A.[88] Galactose can also selectively bind to C-type lectin receptors on alveolar macrophages[87] and carbohydrate receptors on E. coli cells.[89] Carbohydrates, in particular glycoconjugates, play an essential role in cancer metastasis and communication, through the interaction with endogenous lectins present on the cancer cells.[90,91] Galectins (galactose binding lectins), are found to be overexpressed on cancer malignant cells.[92,93] Galectins have been reported as indicators for malignancies in stomach,[94] liver,[95] and colon cancer.[96–98] Glucose transporters (GLUTs) at the blood-brain barrier maintain the continuous high glucose and energy demands of the brain and thus glucose can be used to enhance the translocation of nanoparticles across the blood-brain barrier.[99] N-Acetylglucosamine (GlcNAc) is a component of glycoproteins, proteoglycans, GAGs (glycosaminoglycans) and bacterial and fungal cell walls and it can be applied to induce immunity responses.[100] Furthermore, N-acetylgalactosamine (GalNAc) α-glycosilation to threonine or serine is included in the Tn antigen, one of the most specific human tumor- associated carbohydrate antigen.[101,102]

Efforts to equip penetrating peptides with glycan pendants (e.g. galactose) have shown a reduction of the penetration efficiency together with enhanced viability of the targeted cells.[103] However, these interesting seminal studies with glycosylated penetrating peptides were restricted to the galactose pendant and the *chinese hamster ovary* cell line.[32] Recently, penetrating polydisulfides (**GCPDs**) have also been prepared with glycan moieties to enhance solubility of the resulting polymer conjugates.[104] Nevertheless, to date there is no a systematic study on the properties of different glycosylated penetrating peptides. In this work we have developed a suitable synthetic convergent strategy for the preparation and systematic evaluation of the uptake efficiency and intracellular distribution of glycosylated peptides in different cell lines. For this purpose we have designed an amphiphilic peptide scaffold that incorporates two reactive alkoxyamine connectors[3,105,106] to anchor glycan aldehydes (Fig. 1A). After glycan oxime connection, we studied the impact over the secondary structure and the internalization efficiency of the corresponding glycopeptides. The resulting peptide hybrids showed differences in their secondary structure and in their membrane translocation efficiency depending on the glycan moiety and the different cell lines tested. The results described here highlight the importance and the potential and of peptide glycosylation for adjusting the penetrating efficiency and cytoxicity of glycosylated cell penetrating peptides, **GCPPs**.

Results and Discussion

Design and synthesis. Recent studies established the influence of guanidinium distribution in the delivery properties of penetrating peptides.[107] Therefore, we have designed a linear peptide sequence that would lead to an α-helical amphiphilic folded peptide.[108,109] In this design, we have included the

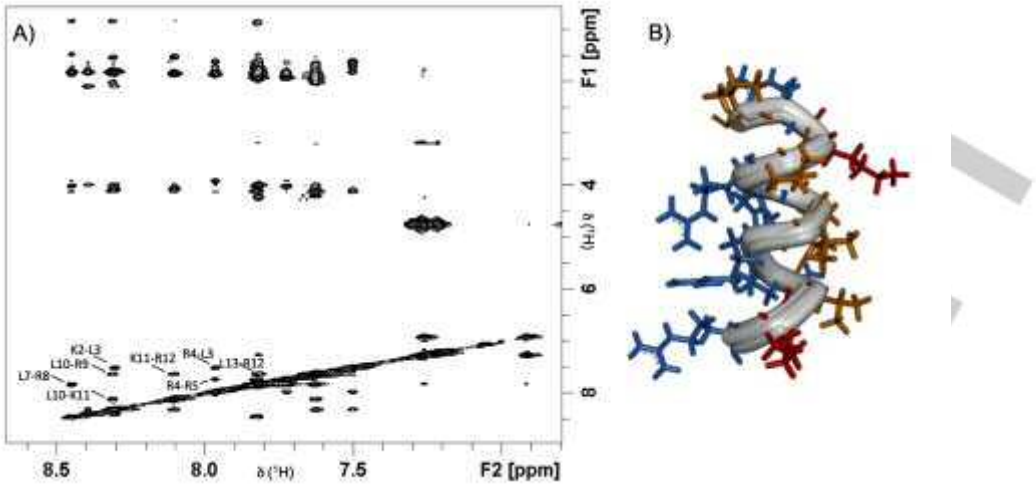

Figure 3. A) 2D NOESY spectrum of the peptide (Ac**P**(Man)$_2$) containing mannose acquired in phosphate buffer 20 mM containing 10% D_2O and 30% TFE, at 600 MHz. B) Ac**P**(Man)$_2$ peptide structure derived by NMR applying the CYANA software. Color code is: Arg (blue), Leu (orange) and Lys (red).

reactive alkoxyamine pendants at the interphase between the segregated cationic and hydrophobic domains in order to minimize the impact on the secondary structure of the resulting folded peptide (Fig. 1B). Orthogonal positioning of the glycan pendants was selected to study the impact on the peptide secondary structure and to maximize the masking of the amphilicity of the peptide scaffold. The corresponding peptide sequence was synthesized by a solid phase approach using orthogonal protecting groups (see supporting information, Fig. S1). As previously described,[108] we employed lysines protected with the methyltrityl group (Mtt) that can be selectively deprotected using weakly acidic conditions, allowing the possibility of synthetically modifying the peptide while it is still anchored to the resin.[108] After Mtt cleavage and "*on-resin*" alkoxyamine incorporation, the peptides were labeled with a fluorophore (TAMRA) to allow the microscopy and cytometry evaluation of their cellular internalization. Peptides were then cleaved from the solid support and immediately conjugated with different glycans aldehydes.[110] Importantly, this oxime bio-orthogonal conjugation proceeded in water at room temperature and in short times with quantitative yields in most of the cases (Fig. S2). The synthesis of the glycan aldehydes was accomplished by our previously developed synthetic route, which involves a Fischer modified glycosylation strategy with a final ozonolysis step of the O-Allyl pendant at the glycan anomeric position.[37] This strategy allowed the preparation of different glycan aldehydes such as α-D-mannose, β-D-glucose, N-acetyl-β-D-glucosamine, β-D-galactose and a branched tri-saccharide branched aldehyde of α-D-mannose (Fig. 2A).[110] Finally, after peptide/glycan oxime connection, the removal of the excess of the glycan aldehyde was accomplished by high-performance liquid chromatography (HPLC). The final glycopeptides were characterized by mass spectrometry (MS), ^{1}H-NMR and circular dichroism (CD).

The circular dichroism of the resulting glycopeptides was measured in buffer HKR (pH = 7.4) and trifluoroethanol (TFE) and it showed the typical bands of the α-helix at 208 and 222 nm (Fig. 2B and supporting information Fig. S4). By following the band at 222 nm we estimated a percentage of helicity in the range of 30 to 20% in buffered conditions for the different peptides (Fig. 2B). The CD cotton effects of the glycopeptide hybrids slightly varied depending on the particular glycan attached to the peptide scaffolds and the intensity of the bands indicated a modest helical behavior in aqueous conditions. However, this helicity was maintained even at high temperatures (60ºC), an interesting observation especially considering the short length of these glycopeptide conjugates (Fig. 2B). Additionally, in the presence of the non-hydrogen bonding competing and helical promoter trifluoroethanol solvent, the helicity of the peptides was strongly increased up to 60% in the best cases (Fig. 2B and S4). Surprisingly, the more hydrophobic acetone capped control peptide, Tm**P**(Acetone)$_2$, showed the lowest helicity of all the peptides reported in this study in aqueous buffer and HKR (see SI Figure S4). These results suggested that for this particular peptide scaffold, the increased hydrophobicity was detrimental for the helical character and that glycan residues might contribute to peptide helicity stabilization.
Interestingly, the peptide bearing the tri-saccharide branched aldehyde lost the helicity, an observation that could indicate that high levels of glycosylation on small scaffolds could have a strong impact on their secondary structure. To further investigate the helical propensity and the secondary structure in these peptides, we employed NMR for a model peptide in aqueous conditions after the addition of aliquots of TFE solvent. The band at 209 nm of the circular dichroism spectra studied showed differences in intensity and even disappeared and/or coalesced with the band at 222 nm (Fig. 2B). This observation has been reported before for other helical peptides and it has been related with the path length of the quartz cuvette and the relative orientation of helical peptides.[111]

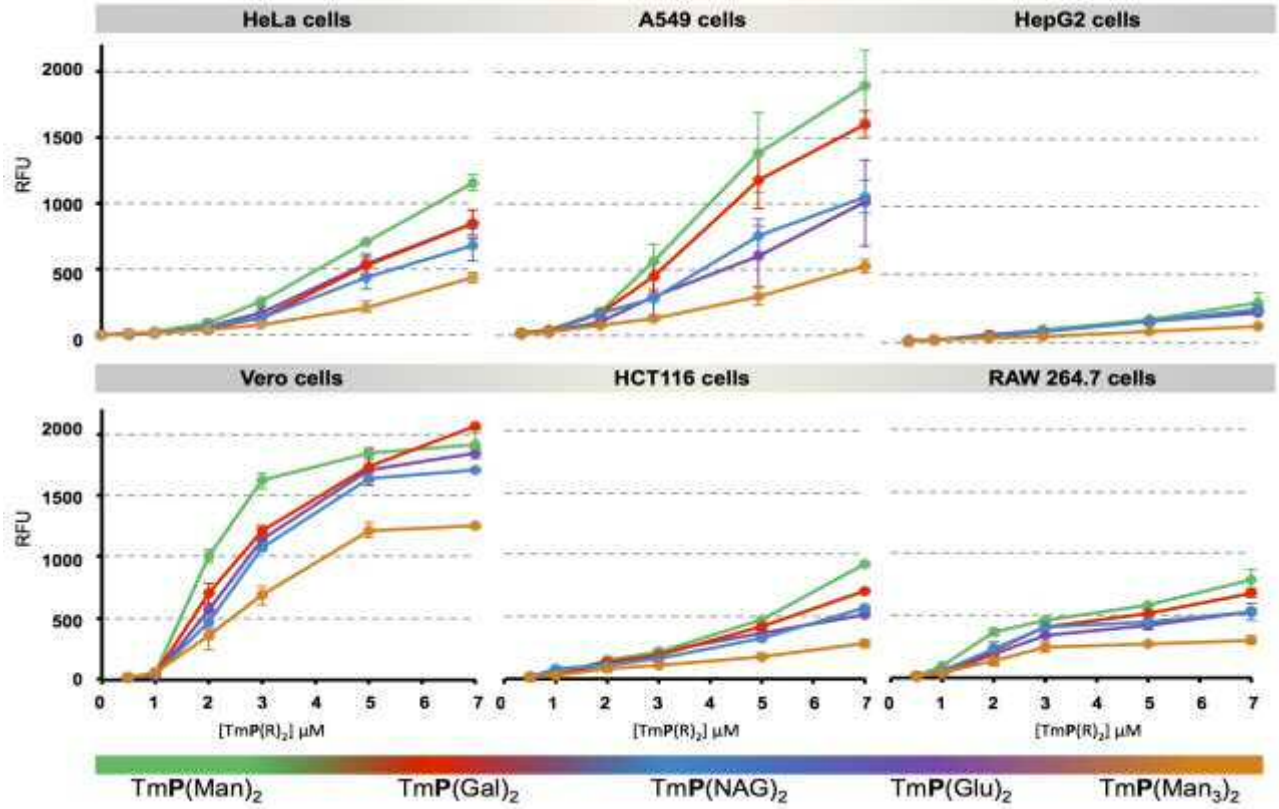

Figure 4. Flow cytometry assay. Internalization efficiency measured by flow cytometry in the different cell lines with Tm**P**$(Man)_2$ (green), Tm**P**$(Gal)_2$ (red), Tm**P**$(NAG)_2$ (blue), Tm**P**$(Glu)_2$ (purple), and Tm**P**$(Man_3)_2$ (orange) at different concentrations (0, 0.1, 0.5, 0.75, 1, 2, 3, 5, 7 μM). RFU in HeLa cells at 3μM of Tm**P**$(Acetone)_2$: 1731.8 ± 432.8.

NMR measurements. These studies were carried out to study in detail the secondary structure of the peptides and support the circular dichroism data of these highly entropic short peptides (Fig. 3). The NMR spectra of the peptide derivative containing two mannoses and acetylated at its N-terminus (Ac**P**$(Man)_2$) were acquired in phosphate buffer in the presence of 30% trifluoroethanol. In these conditions, the spectra showed good signal dispersion and the characteristic Nuclear Overhauser Effects, NOEs, NHi-NHi-1 of helical structures (Fig. 3). Thirty-five inter-residue NOEs could be assigned and converted into distance restraints to calculate the peptide structure with CYANA (see supporting information for details). Figure 3B shows the resulting helical structure displaying segregated domains with the arginine and the leucine residues in the opposite sides of helical longitudinal axis (Fig. 3). The structure of the same peptide containing the fluorescence tag, TAMRA, at $\mathbf{R_1}$ (Tm**P**$(Man)_2$) was also obtained for comparison (Fig. 2A, Fig. S6). In both cases a similar helical structures could be derived from the NMR spectra.

Cellular Internalization Studies. After the synthesis and characterization of the glycosylated cell penetrating peptides (**GCPPs**), we carried out their cellular uptake quantification at different concentrations and in different cell lines. For this evaluation we selected six different cell lines: HeLa (Human cervix adenocarcinoma), A549 (Human lung carcinoma), HepG2 (Human hepatocellular carcinoma), RAW 264.7 (murine macrophage), Vero (Monkey kidney) and HCT116 (Human colorectal carcinoma) (Figs. 4-5). Although we did not intend to perform a detailed glycan/receptor study of glycosylated penetrating peptides, several specific glycan cell receptors are over-expressed in the selected cell lines. For instance, asialoglycoprotein receptor in HepG2 cells, which recognizes galactosyl moieties.[112–114] RAW 264.7 macrophages have shown to bind glycoconjugates that have mannose, N-acetylglucosamine, glucose[115,116] and L-fucose.[117,118] We initially employed flow cytometry to quantify the cellular uptake.[119] In these experiments, peptides were incubated with the cells at different concentrations for 30 minutes, thoroughly washed with medium, trypsinized to remove all membrane bound peptides and the total fluorescence was quantified by cytometry (see supporting information). The results of this internalization experiments are shown in Fig. 4. As expected, due to the different metabolic activity, membrane rigidity and cellular volume, the different cell lines showed very different levels of total internal fluorescence (i.e. compare A549 cells with HepG2 cells, Fig. 4). For instance, all the glycopeptides were very efficiently internalized in Vero and A549 cells, while in RAW 264.7 and HCT116 cells the internalization was intermediate and in the difficult to transfect HepG2 cells the level of uptake was the lowest of the series. In contrast, the pattern of the total internalization in a particular cell line followed a similar trend

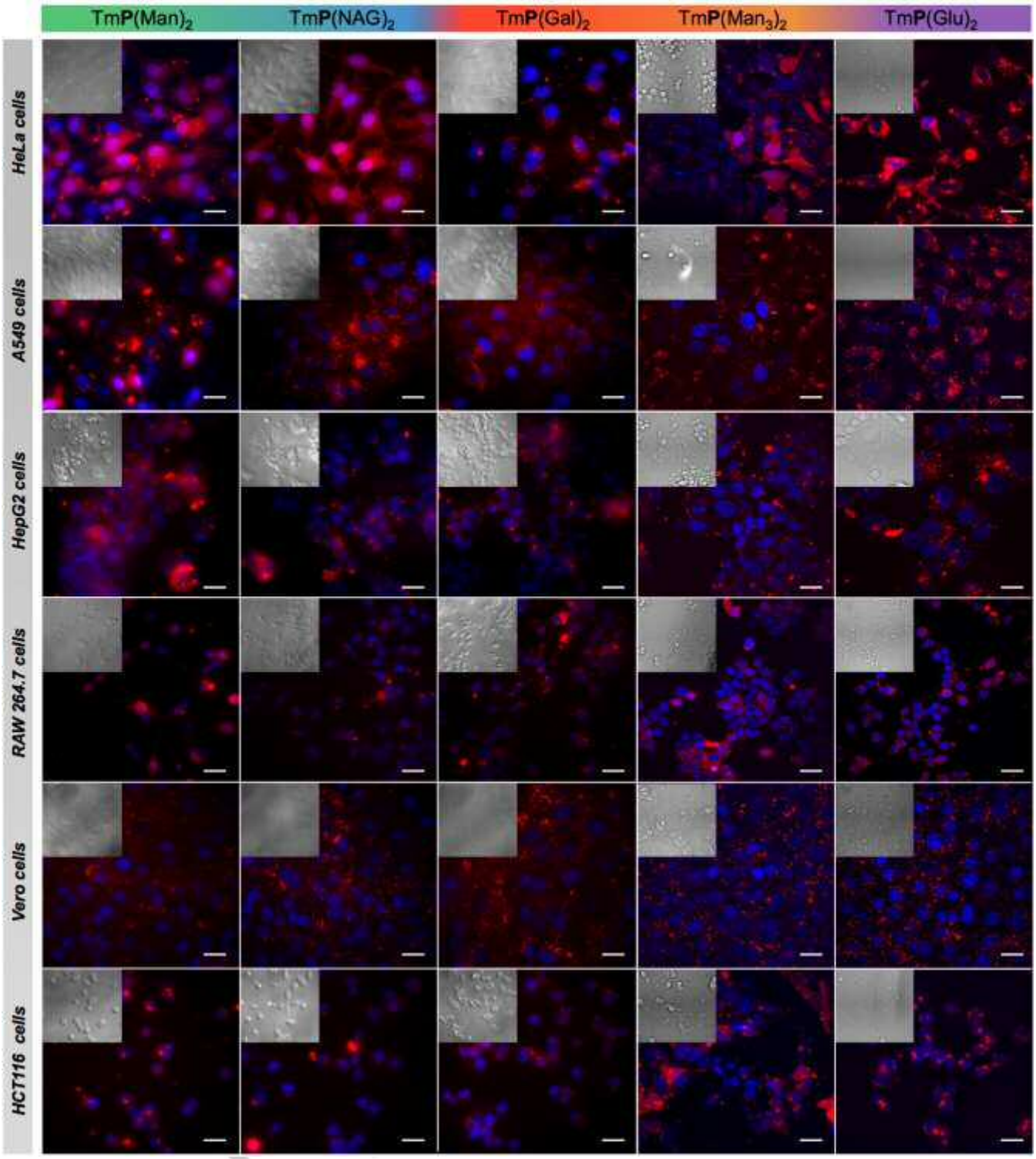

Figure 5. Internalization behavior of each glycopeptides. Series confocal microscopy images of the internalization efficiency of the glycopeptide hybrids reported here. Horizontal lines correspond to the glycopeptides and vertical columns show the different cell lines. Glycopeptides were incubated at 3 μM in HKR buffer during 30 min and 37ºC (see supporting info for details). Scale bar: 25 μm in all cases.

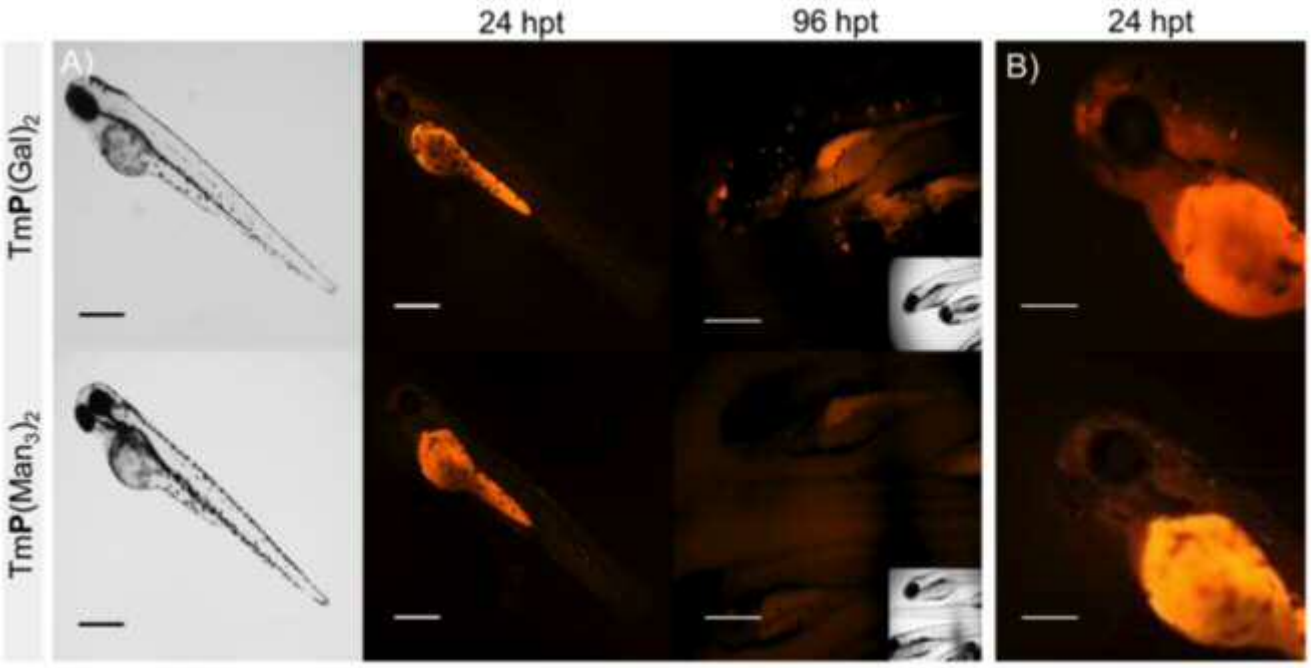

Figure 6. Zebrafish. A) Tm**P**$(Man_3)_2$ and Tm**P**$(Gal)_2$ incubated at 1 μM *in vivo* zebrafish. Horizontal lines show the two glycopeptides and the vertical columns correspond to the hours post-treatment (hpt). After 96 hours no fluorescence can be detected for Tm**P**$(Man_3)_2$ while red dots of the more efficient Tm**P**$(Gal)_2$ can be detected. Scale bar: 500 μm B) Zoom in of the fluorescence images in A after 24 hours, which show specific Tm**P**$(Gal)_2$ localization in the zebrafish head and olfactory placode and the lower signal observed for the Tm**P**$(Man_3)_2$ tri-saccharide. Scale bar: 250 μm in all cases.

depending of the glycan moiety (Fig. 4). In general, the peptides with galactose (Tm**P**$(Gal)_2$) and mannose (Tm**P**$(Man)_2$) showed the highest level of internalization in the different cell lines (Fig. 4). These were followed by glucose and N-acetyl glucosamine that were at a comparable same level in most cases. Finally, the mannose tri-saccharide peptide showed the lowest level of transfection in all the series. The Tm**P**$(Acetone)_2$ control peptide showed the highest penetrating efficiency and we could notice membrane perturbations and higher levels of toxicity for this highly hydrophobic amphiphilic peptide (Fig. S3). We could also confirm by the MTT cytotoxicity assay that the attachment of the glycans to the CPPs scaffold reduced both the cellular toxicity and uptake efficiency of the different glycopeptide hybrids (Fig. S5). Additionally, the confocal dose-response images of Tm**P**$(Acetone)_2$ confirmed the MTT toxicity results, as already at 3 μM concentration of Tm**P**$(Acetone)_2$, the bright field images showed profiled cell nuclei indicating severe toxicity (Fig. S3).

In order to further investigate the internalization and the peptide final intracellular distribution, we next performed a microscopy characterization of the different glycopeptides reported in this study. In these experiments, the glycopeptides were incubated for 30 min at 37ºC with the cells and, before observation, the cells were washed with anionic polymer Heparin in order to reduce the amount of glycopeptide bound to the cell membrane. Cells were then observed by both epifluorescence and confocal microscopy (see supporting info for details). The fluorescent micrographs matched well with the data obtained in the internalization studies performed by cytometry (compare Fig.4 and Fig. 5). The glycopeptides were internalized with distinctive efficiency in the different cell lines and different internalization patterns could be observed for each of the glycopeptides in the micrographs (Fig. 5). We could observe different fluorescence distribution within the same cell line for different glycopeptides. For example, the glycopeptide incorporating the N-acetyl glucosamine (Tm**P**$(NAG)_2$) showed a diffuse internalization pattern in the cell cytosol of HeLa cells, while a punctate fluorescence pattern was observed in the A549 cells at the same glycopeptide concentration (Fig. 5). In addition, the comparison in HeLa cells between the fluorescence pattern of the incorporating N-acetyl glucosamine and galactose respectively (Tm**P**$(NAG)_2$ and Tm**P**$(Gal)_2$) showed a clearly different internalization behavior. While Tm**P**$(NAG)_2$ showed a diffuse cytosolic distribution, the Tm**P**$(Gal)_2$ peptide depicted small aggregates inside the cells suggesting a potential endocytic pathway (Fig. 5). Therefore, the glycans conjugated to the helical peptide scaffold were capable of modulating the penetrating behavior and efficiency of the peptide scaffold. The MTT cytotoxicity studies showed an increased cell viability of certain glycopeptides and a much stronger toxic behaviour of the control peptide Tm**P**$(Acetone)_2$ (Fig. S5). The peptides Tm**P**$(Gal)_2$ and Tm**P**$(NAG)_2$ showed the lowest toxicity of the series, followed by Tm**P**$(Glu)_2$. Intriguingly, the mannose residue showed a slightly higher toxicity than the other glycosylated analogues and the three mannose branched glycan pendant (Tm**P**$(Man_3)_2$) was the more toxic glycopeptide reported here (Fig. S5). This is interesting as it points out that although glycosylation could be considered a biocompatibilization strategy,

even with the simplest carbohydrate models the toxicity of a glycosylated scaffold with low penetrating efficiency can be strongly increased. Additionally, we have compared internalization experiments by flow cytometry of all glycopeptides in DMEM and in DMEM supplemented with 10% FBS. These experiments showed that the presence of serum reduced the uptake efficacy of the peptide hybrids (Fig. S7). However, dose-response confocal microscopy confirmed that a slight increase of the concentration was sufficient to recover efficient cellular uptake and analogous intracellular distribution of the Tm**P**$(Glu)_2$ and the control peptide Tm**P**$(Acetone)_2$ (Fig. S7).

Zebrafish studies. Finally, in order to investigate the potential *in vivo* behavior and distribution of these glycopeptides, we implemented a zebrafish animal model (Fig. 6). We selected the two different peptide examples in terms of uptake efficiency in cells: the galactose bearing peptide Tm**P**$(Gal)_2$ (high uptake) and the mannose tri-saccharide glycopeptide Tm**P**$(Man_3)_2$ (low uptake) to study their distribution *in vivo* in a zebrafish animal model. We thus performed an incubation of post fertilization (hpf) zebrafish larvae in Tm**P**$(Gal)_2$ or Tm**P**$(Man_3)_2$ for 96 hours at 28.5 ºC in static conditions (see supporting info for details). Peptide solutions were evaluated for visualizations at 1 μM and photographing after 24 and 96 hours and the zebrafish was washed prior to observations. Internalization of the glycopeptides was observed at 1 μM without important effects on larval survival (Fig. 6). The strongest signalling appeared at 24 hours post treatment (hpt), mainly in the yolk, whereas a weak fluorescence was detected along the body. In addition, in the tail region, fluorescent dots can be view in the surroundings of caudal artery and vein and in the caudal hematopoietic tissue (CHT) (Fig. 6). At 24 hpt, fluorescence was mainly located at the digestive tract. The pure TAMRA fluorophore did not show any internalization in the zebrafish embryo (24 hours post treatment, Fig. S8). The hydrophobic control peptide Tm**P**$(Acetone)_2$ showed strong internalization in the embryo yolk at short incubations times (24 hours). However, at this concentration (1 μM) Tm**P**$(Acetone)_2$ was not able to leave the yolk even at 96 hours post treatment (Fig. S8). Higher concentrations of this peptide (> 3 μM) showed very strong zebrafish morbidity even at short times (i.e. 24 hours). On the other hand, some differences in fluorescence patterns were distinguished between the two peptides Tm**P**$(Man_3)_2$ (low uptake in cells) and Tm**P**$(Gal)_2$ (higher uptake in cells). At 24 hpt, the mannose tri-saccharide peptide was detected in the larval surface in a regular distribution, which is coincidental with neuromasts (mechanoreceptive organ belonging to the lateral line of the fish (Fig. 6A).[120] However, the galactose peptide generally translocate into the larval body and, specifically, into the zebrafish olfactory placode (Fig. 6B). In addition to the lack of translocation, the fluorescence signal of the mannose tri-saccharide peptide (Tm**P**$(Man_3)_2$) was rapidly cleared from the animal (Fig. 6A 96 hpt). However, the fluorescent dots corresponding to the galactose peptide Tm**P**$(Gal)_2$ were visible even after 96 hpt and distributed in the nasal cavity and musculature of the zebra fish. Therefore, we can conclude that the peptide bearing the galactose pendants with higher internalization efficiency in cell models was also more efficiently translocated and retained into different places of the zebra fish body (Fig. 6).

Conclusions

The objective of this work was not to investigate in detail the potential interactions of glycopeptides with cell membrane receptors or to carry out a detailed internalization mechanistic analysis of these peptide hybrids. Instead, the main target of this work was to demonstrate the potential of the oxime bond connection for the convergent preparation of peptide conjugates with different glycan moieties and to give a broad overview on the effects of their internalization efficiency and distribution in cells. In this regard, the results reported here constitute the first systematic analysis and comparison of the cellular internalization properties of glycopeptide hybrids with different biological relevant glycans attached to a common penetrating peptide template. The most important conclusion of this study is that different glycans have a strong impact on the internalization of the similar peptide scaffold in a particular cell line. However, this study has showed that the trend for the internalization of the glycopeptide hybrids did not change depending on the different cell lines tested. In other words, we did not identify a particular glycopeptide hybrid that was selectively internalized in a particular cell line. In this regard, it seems that penetrating capacity of the peptide scaffold overcomes the glycan potential membrane mediated receptor internalization. However, we can also conclude that the glycan residues modulate the uptake efficiency and the cytotoxicity of a particular peptide sequence in a particular cell line. These results demonstrate that glycosylation of a particular peptide can be used to improve the balance of uptake efficiency and toxicity of glycosylated cell penetrating peptides **GCPPs**.

Acknowledgements

We acknowledge funding from the Spanish Agencia Estatal de Investigación (AEI) [CTQ2014-59646-R, SAF2017-89890-R, CTQ2016-76263-P, CTQ2015-64597-C2-2P], the Xunta de Galicia (ED431G/09, ED431C 2017/25 and 2016-AD031) and the ERDF. I. G. received a predoctoral fellowship from the Xunta de Galicia (ED481A-2018/116). A. R. received a predoctoral fellowship from the Fundación Segundo Gil Dávila. J.G.-V. and L.S. acknowledge the financial support received from the Xunta de Galicia (Galicia, Spain) under the Grupos de Referencia Competitiva Programme: Project GRC2014/010. J. M. received a Ramón y Cajal (RYC-2013-13784), an ERC Starting Investigator Grant (DYNAP-677786) and a Young Investigator Grant from the HFSP (RGY0066/2017).

Keywords: penetrating peptides • peptide synthesis • glycosylation • cell delivery

[1] N. C. Hartman, J. T. Groves, *Curr. Opin. Cell Biol.* **2011**, *23*, 370–376.
[2] D. Schmidt, Q.-X. Jiang, R. MacKinnon, *Nature* **2006**, *444*, 775–779.
[3] A. Fuertes, M. Juanes, J. R. Granja, J. Montenegro, *Chem. Commun.* **2017**, *53*, 7861–7871.
[4] K. M. Stewart, K. L. Horton, S. O. Kelley, *Org. Biomol. Chem.* **2008**, *6*, 2242–2255.
[5] E. A. Goun, T. H. Pillow, L. R. Jones, J. B. Rothbard, P. A. Wender, *ChemBioChem* **2006**, *7*, 1497–1515.
[6] M. Green, P. M. Loewenstein, *Cell* **1988**, *55*, 1179–1188.
[7] A. D. Frankel, C. O. Pabo, *Cell* **1988**, *55*, 1189–1193.
[8] E. Vivès, P. Brodin, B. Lebleu, *J. Biol. Chem.* **1997**, *272*, 16010–16017.
[9] D. Derossi, A. H. Joliot, G. Chassaing, A. Prochiantz, *J. Biol. Chem.* **1994**, *269*, 10444–10450.
[10] N. Sakai, S. Matile, *J. Am. Chem. Soc.* **2003**, *125*, 14348–14356.
[11] T. Takeuchi, M. Kosuge, A. Tadokoro, Y. Sugiura, M. Nishi, M. Kawata, N. Sakai, S. Matile, S. Futaki, *ACS Chem. Biol.* **2006**, *1*, 299–303.
[12] H. D. Herce, A. E. Garcia, M. C. Cardoso, *J. Am. Chem. Soc.* **2014**, *136*, 17459–17467.
[13] F. Duchardt, M. Fotin-Mleczek, H. Schwarz, R. Fischer, R. Brock, *Traffic* **2007**, *8*, 848–866.
[14] D. J. Mitchell, D. T. Kim, L. Steinman, C. G. Fathman, J. B. Rothbard, *J. Pept. Res.* **2000**, *56*, 318–325.
[15] P. A. Wender, D. J. Mitchell, K. Pattabiraman, E. T. Pelkey, L. Steinman, J. B. Rothbard, *Proc. Natl. Acad. Sci.* **2000**, *97*, 13003–13008.
[16] J. B. Rothbard, T. C. Jessop, R. S. Lewis, B. A. Murray, P. A. Wendner, *J. Am. Chem. Soc.* **2004**, *126*, 9506–9507.
[17] N. L. Benner, X. Zang, D. C. Buehler, V. A. Kickhoefer, M. E. Rome, L. H. Rome, P. A. Wender, *ACS Nano* **2017**, *11*, 872–881.
[18] L. Peraro, Z. Zou, K. M. Makwana, A. E. Cummings, H. L. Ball, H. Yu, Y. S. Lin, B. Levine, J. A. Kritzer, *J. Am. Chem. Soc.* **2017**, *139*, 7792–7802.
[19] L. Peraro, K. L. Deprey, M. K. Moser, Z. Zou, H. L. Ball, B. Levine, J. A. Kritzer, *J. Am. Chem. Soc.* **2018**, *140*, 11360–11369.
[20] L. Peraro, J. A. Kritzer, *Angew. Chemie Int. Ed.* **2018**, *57*, 11868–11881.
[21] A. Méndez Ardoy, I. Lostalé-Seijo, J. Montenegro, *ChemBioChem* **2018**, DOI 10.1002/cbic.201800390.
[22] M. C. Morris, J. Depollier, J. Mery, F. Heitz, G. Divita, *Nat. Biotechnol.* **2001**, *19*, 1173–1176.
[23] D. Bhunia, P. Mondal, G. Das, A. Saha, P. Sengupta, J. Jana, S. Mohapatra, S. Chatterjee, S. Ghosh, *J. Am. Chem. Soc.* **2018**, *140*, 1697–1714.
[24] Y. Azuma, H. Imai, Y. Kawaguchi, I. Nakase, H. Kimura, S. Futaki, *Angew. Chemie Int. Ed.* **2018**, *57*, 12771–12774.
[25] W. B. Kauffman, S. Guha, W. C. Wimley, *Nat. Commun.* **2018**, *9*, 2568.
[26] Y. A. Fillon, J. P. Anderson, J. Chmielewski, *J. Am. Chem. Soc.* **2005**, *127*, 11798–11803.
[27] N. W. Luedtke, P. Carmichael, Y. Tor, *J. Am. Chem. Soc.* **2003**, *125*, 12374–12375.
[28] K. K. Maiti, O.-Y. Jeon, W. S. Lee, D.-C. Kim, K.-T. Kim, T. Takeuchi, S. Futaki, S.-K. Chung, *Angew. Chemie Int. Ed.* **2006**, *45*, 2907–2912.
[29] N. Umezawa, M. A. Gelman, M. C. Haigis, R. T. Raines, S. H. Gellman, *J. Am. Chem. Soc.* **2002**, *124*, 368–369.
[30] P. Zhou, M. Wang, L. Du, G. W. Fisher, A. Waggoner, D. H. Ly, *J. Am. Chem. Soc.* **2003**, *125*, 6878–6879.
[31] H.-H. Chung, G. Harms, C. Min Seong, B. H. Choi, C. Min, J. P. Taulane, M. Goodman, *Biopolymers* **2004**, *76*, 83–96.
[32] R. Ni, Y. Chau, *Angew. Chemie Int. Ed.* **2017**, *56*, 9356–9360.
[33] R. Ni, Y. Chau, *J. Am. Chem. Soc.* **2014**, *136*, 17902–17905.
[34] K. Petkau-Milroy, M. H. Sonntag, A. H. A. M. Van Onzen, L. Brunsveld, *J. Am. Chem. Soc.* **2012**, *134*, 8086–8089.
[35] C. J. McKinlay, J. R. Vargas, T. R. Blake, J. W. Hardy, M. Kanada, C. H. Contag, P. A. Wender, R. M. Waymouth, *Proc. Natl. Acad. Sci.* **2017**, *114*, E448–E456.
[36] J. M. Priegue, I. Lostalé-Seijo, D. Crisan, J. R. Granja, F. Fernández-Trillo, J. Montenegro, *Biomacromolecules* **2018**, *19*, 2638–2649.
[37] J. M. Priegue, D. N. Crisan, J. Martínez-Costas, J. R. Granja, F. Fernandez-Trillo, J. Montenegro, *Angew. Chemie Int. Ed.* **2016**, *55*, 7492–7495.
[38] E. Bartolami, C. Bouillon, P. Dumy, S. Ulrich, *Chem. Commun.* **2016**, *52*, 4257–4273.
[39] E. Bartolami, Y. Bessin, V. Gervais, P. Dumy, S. Ulrich, *Angew. Chemie Int. Ed.* **2015**, *54*, 10183–10187.
[40] J. Iriondo-Alberdi, K. Laxmi-Reddy, B. Bouguerne, C. Staedel, I. Huc, *ChemBioChem* **2010**, *11*, 1679–1685.
[41] L. Qian, J. Fu, P. Yuan, S. Du, W. Huang, L. Li, S. Q. Yao, *Angew. Chemie Int. Ed.* **2018**, *57*, 1532–1536.
[42] D. Abegg, G. Gasparini, D. G. Hoch, A. Shuster, E. Bartolami, S. Matile, A. Adibekian, *J. Am. Chem. Soc.* **2017**, *139*, 231–238.
[43] E. Derivery, E. Bartolami, S. Matile, M. Gonzalez-Gaitan, *J. Am. Chem. Soc.* **2017**, *139*, 10172–10175.
[44] G. Gasparini, E.-K. Bang, G. Molinard, D. V. Tulumello, S. Ward, S. O. Kelley, A. Roux, N. Sakai, S. Matile, *J. Am. Chem. Soc.* **2014**, *136*, 6069–6074.
[45] K. Najjar, A. Erazo-Oliveras, J. W. Mosior, M. J. Whitlock, I. Rostane, J. M. Cinclair, J.-P. Pellois, *Bioconjug. Chem.* **2017**, *28*, 2932–2941.
[46] A. Erazo-Oliveras, K. Najjar, L. Dayani, T.-Y. Wang, G. A. Johnson, J.-P. Pellois, *Nat. Methods* **2014**, *11*, 861–867.
[47] M. Akishiba, T. Takeuchi, Y. Kawaguchi, K. Sakamoto, H.-H. Yu, I. Nakase, T. Takatani-Nakase, F. Madani, A. Gräslund, S. Futaki, *Nat. Chem.* **2017**, *9*, 751–761.
[48] I. Lostalé-Seijo, I. Louzao, M. Juanes, J. Montenegro, *Chem. Sci.* **2017**, *8*, 7923–7931.
[49] D. M. Copolovici, K. Langel, E. Eriste, Ü. Langel, *ACS Nano* **2014**, *8*, 1972–1994.
[50] I. Lostalé-Seijo, J. Montenegro, *Nat. Rev. Chem.* **2018**, *2*, 258–277.
[51] C. Gehin, J. Montenegro, E.-K. Bang, A. Cajaraville, S. Takayama, H. Hirose, S. Futaki, S. Matile, H. Riezman, *J. Am. Chem. Soc.* **2013**, *135*, 9295–9298.
[52] J. Yang, A. Bahreman, G. Daudey, J. Bussmann, R. C. L. Olsthoorn, A. Kros, *ACS Cent. Sci.* **2016**, *2*, 621–630.
[53] E. E. Oude Blenke, J. van den Dikkenberg, B. van Kolck, A. Kros, E. Mastrobattista, *Nanoscale* **2016**, *8*, 8955–8965.
[54] L. Adamiak, M. A. Touve, C. L. M. LeGuyader, N. C. Gianneschi, *ACS Nano* **2017**, *11*, 9877–9888.
[55] U. Rothbauer, K. Zolghadr, S. Tillib, D. Nowak, L. Schermelleh, A. Gahl, N. Backmann, K. Conrath, S. Muyldermans, M. C. Cardoso, et al., *Nat. Methods* **2006**, *3*, 887–889.
[56] H. D. Herce, D. Schumacher, A. F. L. Schneider, A. K. Ludwig, F. A. Mann, M. Fillies, M.-A. Kasper, S. Reinke, E. Krause, H. Leonhardt, et al., *Nat. Chem.* **2017**, *9*, 762–771.
[57] S. A. Bode, I. C. Kruis, H. P. J. H. M. Adams, W. C. Boelens, G. J. M. Pruijn, J. C. M. van Hest, D. W. P. M. Löwik, *ChemBioChem* **2017**, *18*, 185–188.
[58] S. A. Bode, S. B. P. E. Timmermans, S. Eising, S. P. W. van Gemert, K. M. Bonger, D. W. P. M. Löwik, *Chem. Sci.* **2019**, DOI 10.1039/C8SC04394A.
[59] P. M. Fischer, *Med. Res. Rev.* **2007**, *27*, 755–795.
[60] D. Kalafatovic, E. Giralt, *Molecules* **2017**, *22*, 1929.
[61] G. Guidotti, L. Brambilla, D. Rossi, *Trends Pharmacol. Sci.* **2017**, *38*, 406–424.
[62] W. B. Kauffman, T. Fuselier, J. He, W. C. Wimley, *Trends Biochem. Sci.* **2015**, *40*, 749–764.
[63] T. Johannssen, B. Lepenies, *Trends Biotechnol.* **2017**, *35*, 334–346.
[64] N. Soni, N. Soni, H. Pandey, R. Maheshwari, P. Kesharwani, R. K. Tekade, *J. Colloid Interface Sci.* **2016**, *481*, 107–116.
[65] J. Zhao, K. Babiuch, H. Lu, A. Dag, M. Gottschaldt, M. H. Stenzel, *Chem. Commun.* **2014**, *50*, 15928–15931.
[66] C. Englert, M. Pröhl, J. A. Czaplewska, C. Fritzsche, E. Preußger, U. S. Schubert, A. Traeger, M. Gottschaldt, *Macromol. Biosci.* **2017**, *17*, 1600502.
[67] A. Jain, A. Agarwal, S. Majumder, N. Lariya, A. Khaya, H. Agrawal, S. Majumdar, G. P. Agrawal, *J. Control. Release* **2010**, *148*, 359–367.
[68] J. J. Reina, A. Di Maio, J. Ramos-Soriano, R. C. Figueiredo, J. Rojo, *Org. Biomol. Chem.* **2016**, *14*, 2873–2882.
[69] A. Ardá, J. Jiménez-Barbero, *Chem. Commun.* **2018**, *54*, 4761–4769.
[70] L. Kong, A. Almond, H. Bayley, B. G. Davis, *Nat. Chem.* **2016**, *8*, 461–469.
[71] B. G. Davis, M. A. Robinson, *Curr. Opin. Drug Discov. Devel.* **2002**, *5*, 279–88.
[72] W. Wu, R. Tang, Q. Li, Z. Li, *Chem. Soc. Rev.* **2015**, *44*, 3997–4022.
[73] L. Cai, Z. Gu, J. Zhong, D. Wen, G. Chen, L. He, J. Wu, Z. Gu, *Drug Discov. Today* **2018**, *23*, 1126–1138.
[74] W. Peng, J. C. Paulson, *J. Am. Chem. Soc.* **2017**, *139*, 12450–12458.
[75] V. N. Tra, D. H. Dube, *Chem. Commun.* **2014**, *50*, 4659–4673.
[76] Y. F. Tan, L. L. Lao, G. M. Xiong, S. Venkatraman, *J. Control. Release* **2018**, *284*, 39–48.
[77] E. Dosekova, J. Filip, T. Bertok, P. Both, P. Kasak, J. Tkac, *Med. Res. Rev.* **2017**, *37*, 514–626.
[78] B. Kang, P. Okwieka, S. Schöttler, S. Winzen, J. Langhanki, K.

Mohr, T. Opatz, V. Mailänder, K. Landfester, F. R. Wurm, *Angew. Chemie Int. Ed.* **2015**, *54*, 7436–7440.
[79] D. Straßburger, N. Stergiou, M. Urschbach, H. Yurugi, D. Spitzer, D. Schollmeyer, E. Schmitt, P. Besenius, *ChemBioChem* **2018**, *19*, 912–916.
[80] D. Benito-Alifonso, S. Tremel, B. Hou, H. Lockyear, J. Mantell, D. J. Fermin, P. Verkade, M. Berry, M. C. Galan, *Angew. Chemie - Int. Ed.* **2014**, *53*, 810–814.
[81] N. Kawasaki, J. L. Vela, C. M. Nycholat, C. Rademacher, A. Khurana, N. van Rooijen, P. R. Crocker, M. Kronenberg, J. C. Paulson, *Proc. Natl. Acad. Sci.* **2013**, *110*, 7826–7831.
[82] J. J. García-Vallejo, M. Ambrosini, A. Overbeek, W. E. van Riel, K. Bloem, W. W. J. Unger, F. Chiodo, J. G. Bolscher, K. Nazmi, H. Kalay, et al., *Mol. Immunol.* **2013**, *53*, 387–397.
[83] M. Sánchez-Navarro, A. Muñoz, B. M. Illescas, J. Rojo, N. Martín, *Chem. - A Eur. J.* **2011**, *17*, 766–769.
[84] O. Engström, A. Muñoz, B. M. Illescas, N. Martín, R. Ribeiro-Viana, J. Rojo, G. Widmalm, *Org. Biomol. Chem.* **2015**, *13*, 8750–8755.
[85] T. B. Geijtenbeek, R. Torensma, S. J. van Vliet, G. C. . van Duijnhoven, G. J. Adema, Y. van Kooyk, C. G. Figdor, *Cell* **2000**, *100*, 575–585.
[86] O. Martínez-Ávila, K. Hijazi, M. Marradi, C. Clavel, C. Campion, C. Kelly, S. Penadés, *Chem. - A Eur. J.* **2009**, *15*, 9874–9888.
[87] J. E. Vela Ramirez, R. Roychoudhury, H. H. Habte, M. W. Cho, N. L. B. Pohl, B. Narasimhan, *J. Biomater. Sci. Polym. Ed.* **2014**, *25*, 1387–1406.
[88] S. Wu, X. Huang, X. Du, *Angew. Chemie Int. Ed.* **2013**, *52*, 5580–5584.
[89] G. Yu, Y. Ma, C. Han, Y. Yao, G. Tang, Z. Mao, C. Gao, F. Huang, *J. Am. Chem. Soc.* **2013**, *135*, 10310–10313.
[90] S. Hakomori, *Proc. Natl. Acad. Sci.* **2002**, *99*, 10231–10233.
[91] H. Lis, N. Sharon, *Chem. Rev.* **1998**, *98*, 637–674.
[92] A. Danguy, I. Camby, R. Kiss, *Biochim. Biophys. Acta - Gen. Subj.* **2002**, *1572*, 285–293.
[93] F. T. Liu, G. A. Rabinovich, *Nat. Rev. Cancer* **2005**, *5*, 29–41.
[94] P. Salvatore, C. Contursi, G. Benvenuto, C. B. Bruni, L. Chiariotti, *FEBS Lett.* **1995**, *373*, 159–163.
[95] D. K. Hsu, C. A. Dowling, K. C. G. Jeng, J. T. Chen, R. Y. Yang, F. T. Liu, *Int. J. Cancer* **1999**, *81*, 519–526.
[96] G. Benvenuto, M. L. Carpentieri, P. Salvatore, L. Cindolo, C. B. Bruni, L. Chiariotti, *Mol. Cell. Biol.* **1996**, *16*, 2736–2743.
[97] H. L. Schoeppner, A. Raz, S. B. Ho, R. S. Bresalier, *Cancer* **1995**, *75*, 2818–2826.
[98] X. Sanjuan, P. Fernandez, A. Castells, V. Castronovo, F. van den Brule, F. Liu, A. Cardesa, E. Campo, *Gastroenterology* **1997**, *113*, 1906–1915.
[99] C. Saraiva, C. Praça, R. Ferreira, T. Santos, L. Ferreira, L. Bernardino, *J. Control. Release* **2016**, *235*, 34–47.
[100] Y. Shibata, I. Honda, J. P. Justice, M. R. Van Scott, R. M. Nakamura, Q. N. Myrvik, *Infect. Immun.* **2001**, *69*, 6123–6130.
[101] M. de las Rivas, E. J. Paul Daniel, H. Coelho, E. Lira-Navarrete, L. Raich, I. Compañón, A. Diniz, L. Lagartera, J. Jiménez-Barbero, H. Clausen, et al., *ACS Cent. Sci.* **2018**, *4*, 1274–1290.
[102] I. A. Bermejo, I. Usabiaga, I. Compañón, J. Castro-López, A. Insausti, J. A. Fernández, A. Avenoza, J. H. Busto, J. Jiménez-Barbero, J. L. Asensio, et al., *J. Am. Chem. Soc.* **2018**, *140*, 9952–9960.
[103] L. Dutot, P. Lécorché, F. Burlina, R. Marquant, V. Point, S. Sagan, G. Chassaing, J.-M. Mallet, S. Lavielle, *J. Chem. Biol.* **2010**, *3*, 51–65.
[104] P. Morelli, E. Bartolami, N. Sakai, S. Matile, *Helv. Chim. Acta* **2018**, *101*, e1700266.
[105] I. Louzao, R. García-Fandiño, J. Montenegro, *J. Mater. Chem. B* **2017**, *5*, 4426–4434.
[106] M. Pazo, H. Fernández-Caro, J. Priegue, I. Lostalé-Seijo, J. Montenegro, *Synlett* **2017**, *28*, 924–928.
[107] J. S. Appelbaum, J. R. Larochelle, B. A. Smith, D. M. Balkin, J. M. Holub, A. Schepartz, *Chem. Biol.* **2012**, *19*, 819–830.
[108] M. Juanes, I. Lostalé-Seijo, J. R. Granja, J. Montenegro, *Chem. - A Eur. J.* **2018**, *24*, 10689–10698.
[109] M. Pazo, M. Juanes, I. Lostalé-Seijo, J. Montenegro, *Chem. Commun.* **2018**, *54*, 6919–6922.
[110] J. Reina, A. Rioboo, J. Montenegro, *Synthesis (Stuttg).* **2018**, *50*, 831–845.
[111] E. Biron, N. Voyer, J. Meillon, M.-È. Cormier, M. Auger, *Biopolymers* **2000**, *55*, 364–372.
[112] S. Kawakami, M. Hashida, *J. Control. Release* **2014**, *190*, 542–555.
[113] Q. Wang, L. Zhang, W. Hu, Z. H. Hu, Y. Y. Bei, J. Y. Xu, W. J. Wang, X. N. Zhang, Q. Zhang, *Nanomedicine Nanotechnology, Biol. Med.* **2010**, *6*, 371–381.
[114] K. Jain, P. Kesharwani, U. Gupta, N. K. Jain, *Biomaterials* **2012**, *33*, 4166–4186.
[115] P. D. Stahl, J. S. Rodman, M. J. Miller, P. H. Schlesinger, *Proc. Natl. Acad. Sci. U. S. A.* **1978**, *75*, 1399–1403.
[116] B. L. Largent, K. M. Walton, C. A. Hoppe, Y. C. Lee, R. L. Schnaar, *J. Biol. Chem.* **1984**, *259*, 1764–1769.
[117] J. C. Robbins, M. H. Lam, C. S. Tripp, R. L. Bugianesi, M. M. Ponpipom, T. Y. Shen, *Proc. Natl. Acad. Sci. U. S. A.* **1981**, *78*, 7294–7298.
[118] S. A. Linehan, L. Martínez-Pomares, S. Gordon, *Microbes Infect.* **2000**, *2*, 279–288.
[119] T. Holm, H. Johansson, P. Lundberg, M. Pooga, M. Lindgren, Ü. Langel, *Nat. Protoc.* **2006**, *1*, 1001–1005.
[120] A. B. Chitnis, D. Dalle Nogare, M. Matsuda, *Dev. Neurobiol.* **2012**, *72*, 234–255.

Glycosylated Cell Penetrating Peptides, GCCPs

Iván Gallego,[a] Alicia Rioboo,[a] Dr. José J. Reina,[a] Bernardo Díaz,[b] Dr. Ángeles Canales,[c] Dr. F. Javier Cañada,[b,c] Dr. Jorge Guerra-Varela,[d] Prof. Laura Sánchez,[d] Dr. Javier Montenegro*[a]

[a] Centro Singular de Investigación en Química Biolóxica e Materiais Moleculares (CIQUS), Departamento de Química Orgánica, Universidade de Santiago de Compostela, Campus Vida, 15782 Santiago de Compostela, Spain. *e-mail: javier.montenegro@usc.es

[b] Centro de Investigaciones Biológicas (CIB) del CSIC, C/Ramiro de Maetzu 9, CP 28040, Madrid.

[c] Departamento de Biología Estructural y Química, Fac. Ciencias Químicas Univ. Complutense de Madrid, Avd/ Complutense s/n, CP. 28040, Madrid.

[d] Departamento de Zooloxía, Xenética e Antropoloxía Física. Facultade de Veterinaria Universidade de Santiago de Compostela, 27002, Lugo, Spain.

Table of Contents

Supporting figures

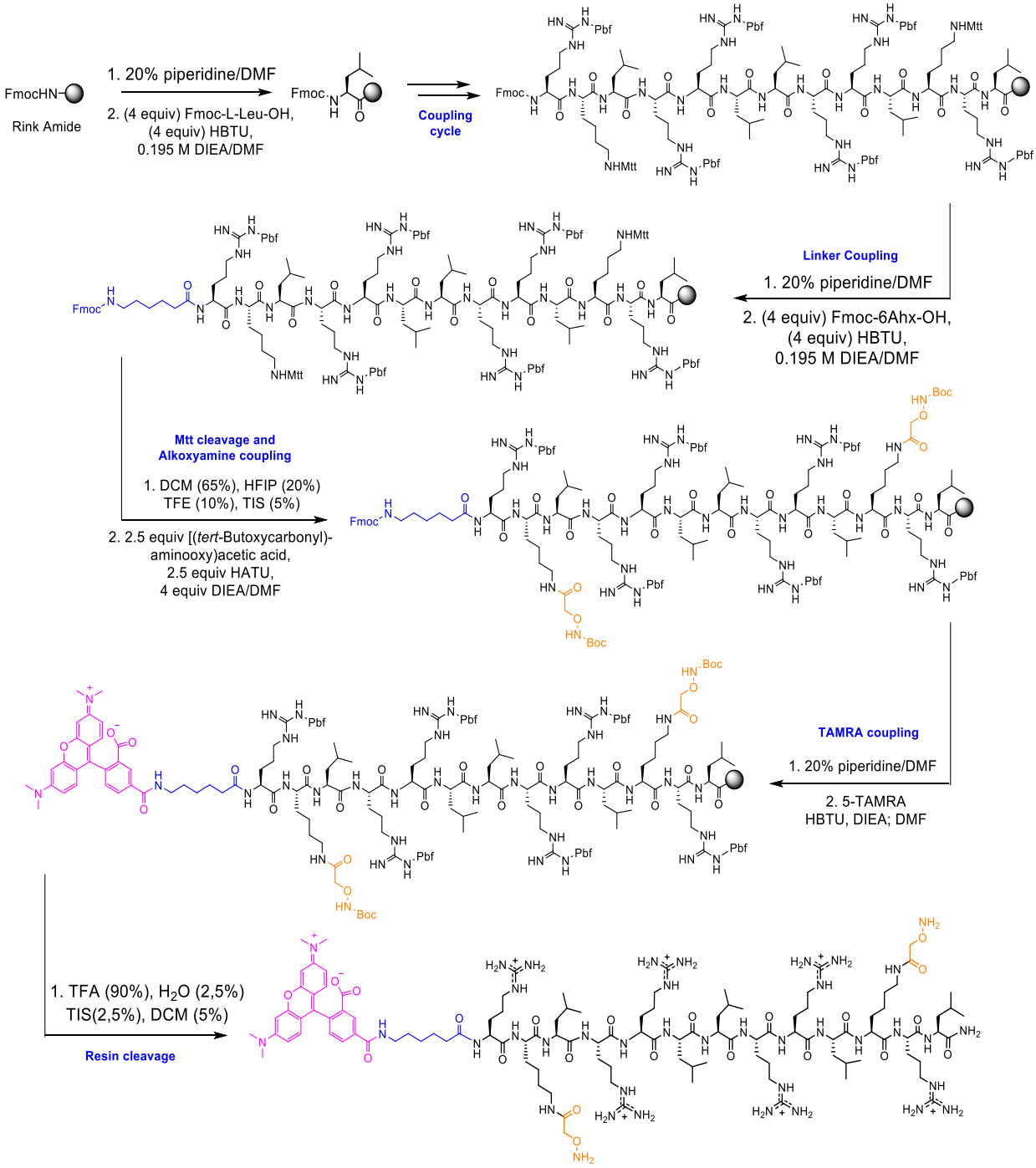

Figure S1. General synthetic scheme for the Solid Phase Peptide Synthesis (SPPS).

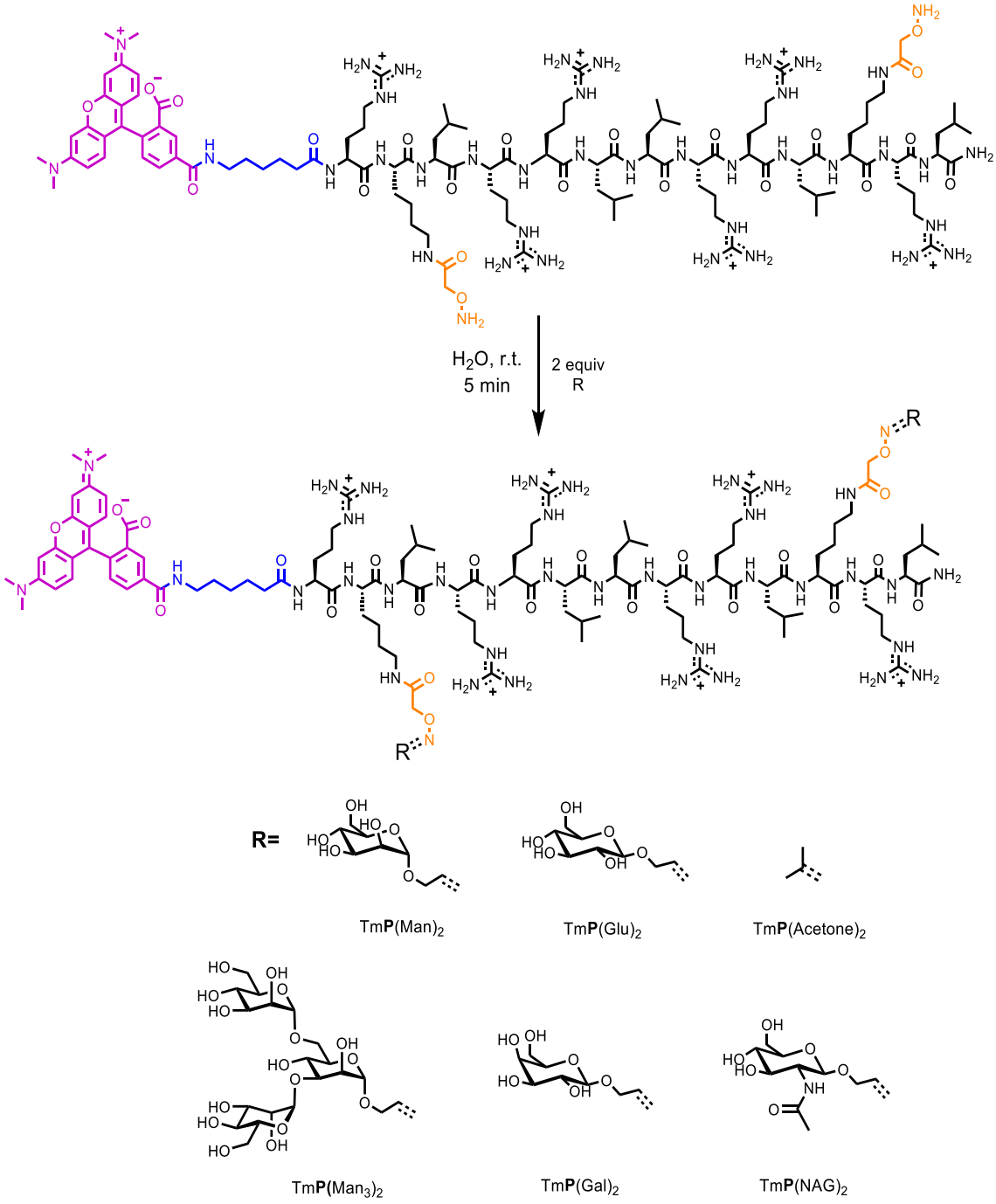

Figure S2. General synthetic scheme for ligands coupling.

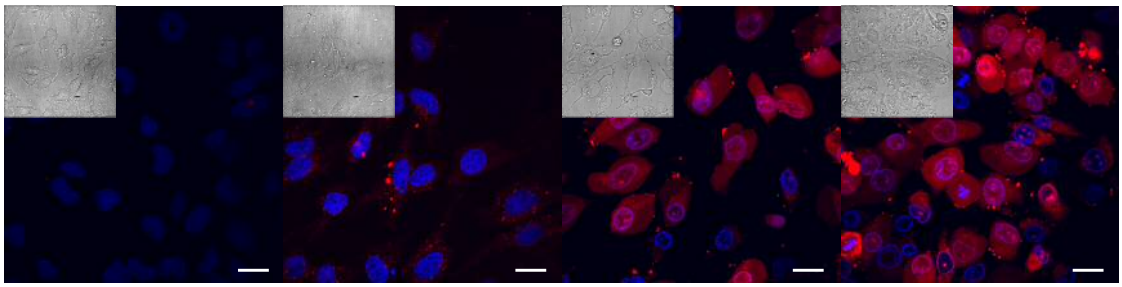

Figure S3. These pictures show a dose-response microscopy images of Tm**P**(Acetone)$_2$ internalization capacity in HeLa cells. (0,5, 1, 3, 5) μM of this control peptide in HKR buffer was incubated for 30 min and 37ºC. Scale bar: 25 μm.

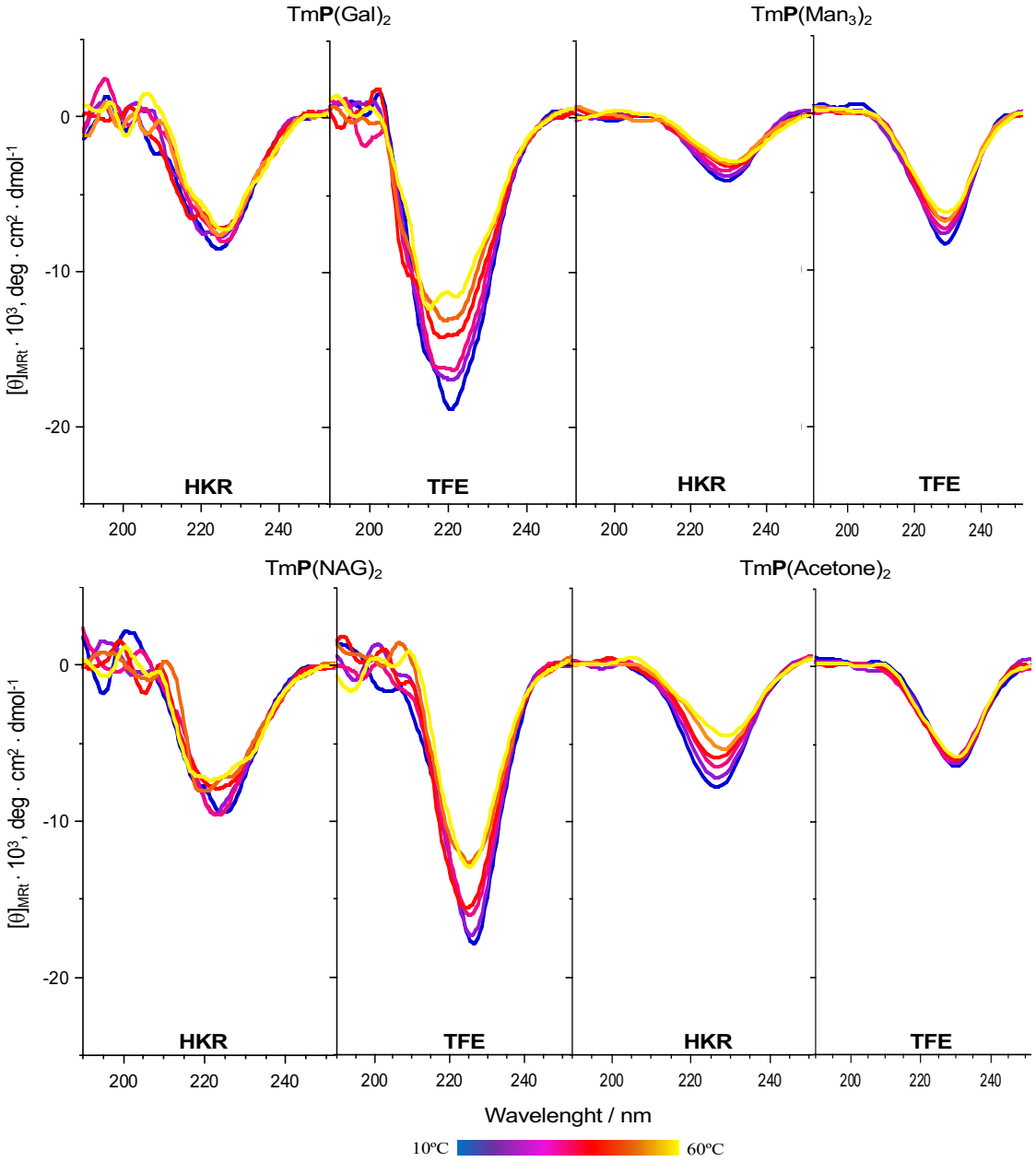

Figure S4. CD spectra of Tm**P**(Gal)$_2$, Tm**P**(NAG)$_2$, Tm**P**(Man$_3$)$_2$ and Tm**P**(Acetone)$_2$ in different conditions, TFE (trifluoroethanol) and HKR buffer (pH 7.4).

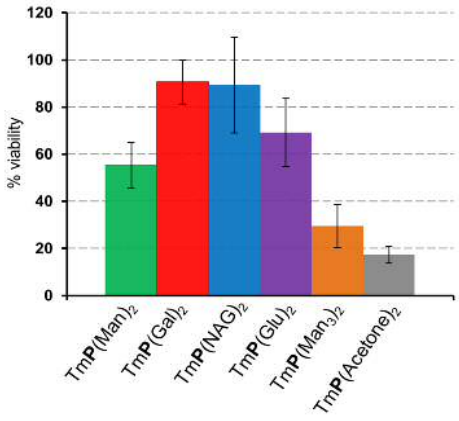

Figure S5. MTT assay. Cytotoxicity of each GCPP and control peptide Tm**P**$(Acetone)_2$ were checked using MTT assay. HeLa cells were incubated at 5 µM during 30 min and 37ºC.

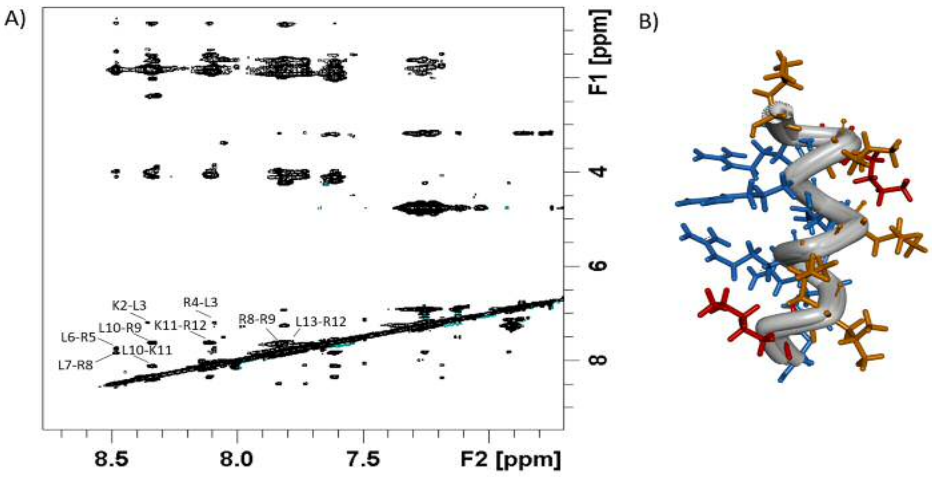

Figure S6. A) 2D NOESY spectrum of Tm**P**$(Man)_2$, acquired in phosphate buffer 20 mM containing 10% D2O and 30% TFE, at 600 MHz. B) Peptide structure by NMR applying the CYANA software.

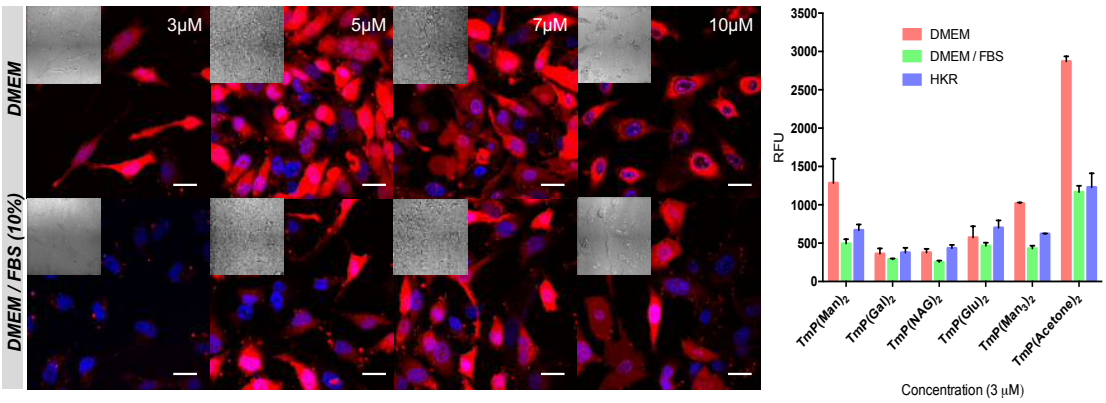

Figure S7. Dose-response microscopy images of Tm**P**$(Glu)_2$ internalization capacity in HeLa cells. (3, 5, 7, 10) μM of this peptide in DMEM and DMEM/FBS (10%) was incubated for 30 min and 37ºC. Scale bar: 25 μm. A) Dose-response confocal experiments. B) Flow cytometry.

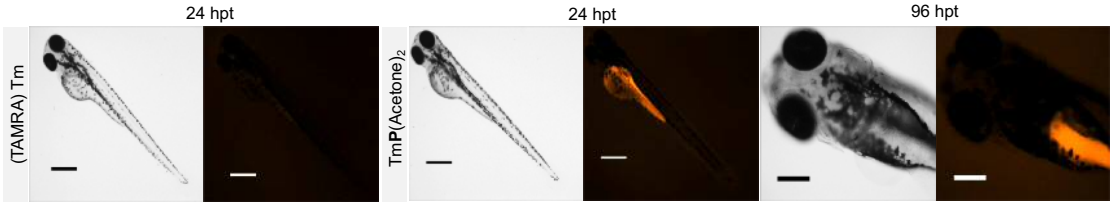

Figure S8. Images of zebra fish showing no fluorescence of the TAMRA control and strong yolk internalization of Tm**P**$(Acetone)_2$ 24 hours post treatment. 96 hours post treatment the Tm**P**$(Acetone)_2$ did not cross the yolk and higher concentrations of this peptide (> 3 μM) showed strong toxicity and complete morbidity to the zebrafish. *In vivo* experiments were performed at 1 μM with Tm (TAMRA) and control peptide Tm**P**$(Acetone)_2$. Scale bar 500 μm (24 hpt) and 250 μm (96 hpt).

Materials and methods

Commercially available Fmoc-Rink Amide AM resin, N-HBTU and Fmoc-L-Lys(Mtt)-OH were used as obtained from Iris. [Tert-butoxycarbonyl)aminooxy]acetic acid were purchased from TCI Chemicals. Fmoc-L-Leu-OH, Fmoc-L-Arg(Pbf)-OH, Fmoc-6Ahx-OH, Heparin sodium salt were purchased from Sigma-Aldrich®. 5(6)-Carboxytetramethlyrhodamine succinimidyl ester were purchased from Carbosynth. Hoechst 33342 Trihydrochloride Trihydrate were purchased in ThermoFisher. Deuterated solvents (D_2O) were from EMD Millipore Corporation. N,N-Dimethylformamide, for peptide synthesis, was purchased from Scharlau. All the other solvents were HPLC grade, purchased from Sigma-Aldrich® or Fisher Scientific® and used without further purification.

High-performance liquid chromatography coupled with mass spectrometry (HPLC-MS) analyses were carried out on Agilent Technologies 1260 Infinity II associated with a 6120 Quadrupole LC-MS using an Agilent SB-C18 column or an DIONEX Ultimate 3000 U-HPLC$^+$ (Thermo Scientific) with an Acclaim RSLC 120-C18 column with Solvent A: Solvent B gradients between 5:95 (Solvent A: H_2O with 0.1% TFA; Solvent B: CH_3CN with 0.1% TFA). High-performance liquid chromatography (HPLC) preparative purification was carried out on Waters 1525 composed by a binary pump with a dual Waters 2489 detector with a Phenomenex Luna C18(2) 100Å column. A JASCO with an Agilent Eclipse XDB-C18 column was used for semi-preparative purification using gradient 5:95 (Solvent A: H_2O with 0.1% TFA; Solvent B: CH_3CN with 0.1% TFA). Nuclear Magnetic Resonance (NMR) spectra were recorded on either a Varian Mercury 300 MHz or a Varian Inova 500 MHz spectrometer. Chemical shifts are reported in ppm (δ

units) referenced to the following solvent signals: D_2O δH 4.79. Spin multiplicities are reported as a singlet (s), doublet (d), triplet (t) with coupling constants (J) given in Hz, or multiplet (m). Accurate mass determinations (HR-MS) using ESI-MS were performed on a Sciex QSTAR Pulsar mass spectrometer and are reported as mass-per-charge ratio (m/z). Recalculation of the labelled peptides concentrations was performed by measuring the absorbance on a Biochrom Libra S60 UV-VIS Spectrophotometer. Circular Dichroism (CD) measurements were performed with a Jasco J-1100 CD Spectrometer equipped with a Jasco MCB-100 Mini Circulation Bath. Cell microscopy images were acquired with an Andor Zyla 4.2 digital camera mounted on a Nikon Eclipse Ti-E epifluorescence microscope and with a Leica SP5 confocal microscope. A Guava EasyCyteTM cytometer (EMD Millipore) was used for all flow cytometry experiments.

Abbreviations

Peptide Abbreviations: Tm**P**$(X)_2$ (Tm = TAMRA and X = Man, Glu, Acetone, Man_3, Gal and NAG); Aa: Amino acid; Arg: Arginine; Boc: tert-Butoxycarbonyl; CPP: Cell-Penetrating Peptide; DCM: Dichloromethane; DIEA: N,N-Diisopropylethylamine; DMF: N,N-Dimethylformamide; FBS: Fetal Bovine Serum; Fmoc: 9-fluorenylmethoxycarbonyl; HFIP: 1,1,1,3,3,3-Hexafluoro-2-propanol; HKR: HEPES-Krebs-Ringer buffer; HRMS (ESI): High resolution mass spectrometry (electrospray ionization); Lys: Lysine; Mtt: 4-Methyltrityl; MTT: 3-(4,5-dimethylthiazol-2-yl)-2,5-diphenyltetrazolium bromide; N-HATU: N-[(Dimethylamino)-1H-1,2,3-triazolo[4,5-b]pyridin-1-ylmethylene]-N-methyl methanaminiun hexafluorophosphate N-oxide; N-HBTU: N-[(1HBenzotriazol-1-yl)4-(dimethylamino)methylene]-N-methyl methanaminiumhexafluoro phosphate N-oxide; Pbf: 2,2,4,6,7-Pentamethyldihydrobenzofuran-5-sulfonyl; RP: Reverse Phase; SPPS: Solid Phase Peptide Synthesis; TAMRA: 5(6)-Carboxytetramethlyrhodamine succinimidyl ester; TFE: Trifluoroethanol; TIS: Triisopropylsilane; TNBS: 2,4,6-Trinitrobenzenesulfonic acid; 6Ahx: 6-aminohexanoic acid. DMEM: Dulbecco's Modified Eagle Medium. FBS: Fetal Bovine Serum.

General protocols

General protocols for the SPPS

All peptides were synthesized by manual Fmoc solid-phase peptide synthesis[1,2] using Rink Amide resin (loading 0.71 mmol/g). The resin (0.1 mmol) was swelled in DMF (peptide synthesis grade, 2 mL) for 20 min in a peptide synthesis vessel prior synthesis. Coupling cycle consisted of the removal of Fmoc protecting group with a solution of piperidine in DMF (20%, 2mL) for 10 min and then the mixture was filtered and the resin was washed with DMF (3x2 mL, 1 min). The amino acid coupling was carried out by treatment with a solution of α-amino acids (4 equiv), N-HBTU (3.95 equiv) in DMF (2 mL), which was mixed with DIEA (0.195 M solution in DMF, 1.2 equiv) 1 min before the addition and the resulting mixture was shaken by bubbling Ar for 15 min. Finally, the resin was washed with DMF (3x2 mL, 1 min). The efficiency of each amino acid coupling and deprotection was monitored employing the TNBS test[3]. Once the linear peptide was finished, the ending protocol used was “linker coupling”, after Fmoc cleavage with piperidine/DMF (20%, 2mL), the linear peptide was treated with a solution of N-Fmoc-6-aminohexanoic acid (4 equiv), N-HBTU (3.95 equiv) and DIEA (0.195 M solution in DMF, 1.2 equiv) in DMF.

The resin was washed with DCM (2x2 mL, 5 min), and the Mtt protecting group was selectively removed by mechanical shaking of the resin with a mixture of DCM/HFIP/TFE/TIS (6.5:2:1:0.5, 2x2 mL, 2 h). Finally, the mixture was filtered and the resin was washed with DCM (2x2 mL, 2

min) and DMF (2 mL, 20 min). A solution of [(tert-butoxycarbonyl) aminooxy] acetic acid (2.5 equiv per free amine) and N-HATU (2.5 equiv) in DMF (1 mL) was added to the resin followed by the dropwise addition of a solution of DIEA (4 equiv) in DMF (0.5 mL). The resin was shaken by bubbling Ar for 30 min and finally washed with DMF (3x2 mL, 2 min) and DCM (3x2 mL, 2 min).

General protocol for N-terminal functionalization

Fluorescently labelled peptides: the Fmoc-protecting group of the previously attached linker was removed by using a solution of piperidine in DMF (20%, 4 mL) for 15 min and the resin was washed with DMF (3x3 mL). The coupling was carried out by the addition of a solution of 5(6)-Carboxytetramethylrhodamine succinimidyl ester (1 equiv) and DIEA (0.195 M, 1 equiv) in DMF (2 mL) and the mixture was stirred by bubbling Ar for 30 min. Finally, the resin was washed with DMF (3x3 mL) and DCM (3x3 mL).

General protocol for peptide cleavage

Finally, peptides were deprotected and cleaved from the resin by standard TFA cleavage procedure at rt by using TFA/DCM/H_2O/TIS (90:5:2.5:2.5, 1 mL per 70 mg of resin) for 2 h. Then, the mixture was filtered, washed with TFA (1 mL) and the peptide was precipitated with ice-cold Et_2O (25 mL). The precipitate was centrifuged and dissolved in H_2O (5 mL). Peptides were obtained following the previously described procedure, and were treated with the different ligands without purification.

General protocol for ligand coupling

A solution of peptide in H_2O (5 mM) was reacted with a solution of corresponding aldehyde ligands[4] (2 equiv. per alkoxyamine) in H_2O (120 mM) for 5 min. Then, peptides were purified by RP-HPLC for removing the ligand excess. The purification was carried by Agilent Eclipse XDB-C18 column H2O (0.1% TFA)/CH_3CN (0.1% TFA), 95:5→5:95 (5→35 min)] with a binary gradient of Solvent A and Solvent B, the collected fractions were lyophilized and stored at -20 °C. Purity and identity were confirmed by HPLC, ^{1}H-NMR and low and high resolution mass spectrometry.

Synthesis of peptides

*Synthesis of Tm**P**$(Man)_2$*

Following the general protocol of the SPPS for synthesizing a TAMRA labelled peptide with two α-D-mannoses, Tm**P**$(Man)_2$ was obtained after RP-HPLC purification [Agilent Eclipse XDB-C18, 9.4x250 mm, H_2O (0.1% TFA)/ CH_3CN (0.1% TFA) 95:5→5:95 (0→35 min)] with an overall yield of 6% (17 mgs) and 99% purity. R_t 7.62 min (Fig. S6) [RP-HPLC Agilent SB-C18 column, H_2O (0.1% TFA)/ CH_3CN (0.1% TFA) 95:5→5:95 (0→12 min)]. The spectroscopic data matched those previously reported.[2] **^{1}H-NMR** (500 MHz, D_2O, δ): 8.21 (s, 1H), 7.92 (d, *J* = 8.1 Hz, 1H), 7.58 (m, 1H), 7.36 (d, *J* = 8.1 Hz, 1H), 7.11 (t, *J* = 9.9 Hz, 2H), 6.97 (m, 1H), 6.83 (d, *J* = 9.6 Hz, 2H), 6.75 (s, 2H), 4.80-4.73 (m, 2H), 4.68 (s, 4H), 4.40 (d, *J* = 24.1 Hz, 4H), 4.28-3.96 (m, 13H), 3.87-3.24 (m, 12H), 3.13 (s, 12H), 3.10-2.95 (m, 16H), 2.91-2.80 (m, 2H), 2.25 (t, *J* = 7.1 Hz, 2H), 1.79-1.11 (m, 57H), 0.87-0.67 (m, 30H). **MS** (ESI, H_2O): 1657 (7, $[M+2H+4TFA]^{+2}$), 1599 (17, $[M+2H+3TFA]^{+2}$), 1542 (15, $[M+2H+2TFA]^{+2}$), 1027 (100, $[M+3H+2TFA]^{+3}$), 989 (99, $[M+3H+TFA]^{+3}$), 953 (28, $[M+3H+]^{+3}$), 743 (62, $[M+4H+TFA]^{+4}$), 716 (53, $[M+4H]^{+4}$). **HRMS** (ESI): Calculated for $C_{129}H_{217}N_{39}O_{34}$: 1428.3220; found: 1428.3209 ($[M+2H]^{+2}$).

*Synthesis of Tm**P**$(Gal)_2$*

Following the general protocol of the SPPS for synthesizing a TAMRA labelled peptide with two β-D-galactoses, Tm**P**$(Gal)_2$ was obtained after RP-HPLC purification [Agilent Eclipse XDB-C18, 9.4x250 mm, H_2O (0.1% TFA)/ CH_3CN (0.1% TFA) 95:5→5:95 (0→35 min)] with an overall yield of 9% (26 mgs) and 97% purity. R_t 7.81 min (Fig. S7) [RP-HPLC Agilent SB-C18 column, H_2O (0.1% TFA)/ CH_3CN (0.1% TFA) 95:5→5:95 (0→12 min)]. **^{1}H-NMR** (500 MHz, D_2O, δ): δ 8.47 (s, 1H), 8.08-7.96 (m, 1H), 7.63-7.53 (m, 1H), 7.25 (s, 1H), 7.06-6.91 (m, 2H), 6.89-6.83 (m, 1H), 6.79-6.62 (m, 2H), 6.57 (s, 2H), 4.81-4.68 (m, 4H), 4.66-4.58 (m, 4H), 4.38 (s, 2H), 4.28-3.90 (m, 13H), 3.89-3.31 (m, 12H), 3.19-3.05 (m,16H), 3.04 (s, 12H), 2.91-2.71 (m, 2H), 2.37-2.11 (m, 2H), 1.98-1.04 (m, 57H), 0.90-0.53 (m, 30H). **MS** (ESI, H_2O): 1599 (7, $[M+2H+3TFA]^{+2}$), 1543 (8, $[M+2H+2TFA]^{+2}$), 1029 (75, $[M+3H+2TFA]^{+3}$), 991 (100, $[M+3H+TFA]^{+3}$), 953 (20, $[M+3H]^{+3}$), 744 (35, $[M+4H+TFA]^{+4}$), **HRMS** (ESI): Calculated for $C_{129}H_{218}N_{39}O_{34}$: 952.5504; found: 952.5499 ($[M+3H]^{+3}$).

*Synthesis of Tm**P**$(NAG)_2$*

Following the general protocol of the SPPS for synthesizing a TAMRA labelled peptide with two N-acetyl-β-D-glucosamine, Tm**P**$(NAG)_2$ was obtained after RP-HPLC purification [Agilent Eclipse XDB-C18, 9.4x250 mm, H_2O (0.1% TFA)/ CH_3CN (0.1% TFA) 95:5→5:95 (0→35 min)] with an overall yield of 9% (26 mgs) and 98% purity. R_t 7.63 min (Fig. S8) [RP-HPLC Agilent SB-C18 column, H_2O (0.1% TFA)/ CH_3CN (0.1% TFA) 95:5→5:95 (0→12 min)]. **^{1}H-NMR** (500 MHz, D_2O, δ): 8.37 (s, 1H), 8.08 (s, 1H), 7.97-7.86 (m, 1H), 7.77 (s, 1H), 7.49 (t, J = 5.4 Hz, 2H), 6.97-6.91 (m, 1H), 6.91-6.81 (m, 2H), 6.67-6.52 (m, 2H), 4.54-4.46 (m, 2H), 4.47-4.32 (m, 19.7 Hz, 4H), 4.29-3.89 (m, 13H), 3.77-3.29 (m, 12H), 3.09 (s, 12H), 3.08-2.95 (m, 16H), 2.85-2.71 (m, 2H), 2.34-2.22 (m, 2H), 1.94-1.85 (m, 6H), 1.81-1.29 (m, 57H), 0.86-0.57 (m, 30H). **MS** (ESI, H_2O): 1638 (10, $[M+2H+3TFA]^{+2}$), 1581 (5, $[M+2H+2TFA]^{+2}$), 1055 (100, $[M+3H+2TFA]^{+3}$), 1016 (80, $[M+3H+TFA]^{+3}$), 979 (15, $[M+3H]^{+3}$),762 (30, $[M+4H+TFA]^{+4}$), 734 (25, $[M+4H]^{+4}$), **HRMS** (ESI): Calculated for $C_{133}H_{224}N_{41}O_{34}$: 979.9014; found: 979.9011 ($[M+3H]^{+3}$).

*Synthesis of Tm**P**$(Glu)_2$*

Following the general protocol of the SPPS for synthesizing a TAMRA labelled peptide with two β-D-glucose, Tm**P**$(Glu)_2$ was obtained after RP-HPLC purification [Agilent Eclipse XDB-C18, 9.4x250 mm, H_2O (0.1% TFA)/ CH_3CN (0.1% TFA) 95:5→5:95 (0→35 min)] with an overall yield of 15% (42 mgs) and 99% purity. R_t 7.59 min (Fig. S9) [RP-HPLC Agilent SB-C18 column, H_2O (0.1% TFA)/ CH_3CN (0.1% TFA) 95:5→5:95 (0→12 min)]. **^{1}H-NMR** (300 MHz, D_2O, δ): 8.21 (s, 1H), 7.96-7.91 (m, 1H), 7.83 (s, 1H), 7.69-7.57 (m, 1H), 7.19-7.12 (m, 2H), 7.09-7.00 (m, 1H), 6.75 (s, 2H), 6.65-6.57 (m, 2H), 4.46 (s, 2H), 4.41-4.33 (m, 4H), 4.27-4.00 (m, 13H), 3.86-3.27 (m, 12H), 3.13 (s, 12H), 3.10-3.02 (m, 16H), 2.76 (d, J = 7.4 Hz, 2H), 2.31-2.18 (m, 2H), 1.96-1.09 (m, 57H), 0.95-0.60 (m, 30H). **MS** (ESI, H_2O): 1598 (10, $[M+2H+3TFA]^{+2}$), 1544 (8, $[M+2H+2TFA]^{+2}$), 1029 (50, $[M+3H+2TFA]^{+3}$), 991 (100, $[M+3H+TFA]^{+3}$), 953 (23, $[M+3H]^{+3}$), 744 (47, $[M+4H+TFA]^{+4}$), 715 (43, $[M+4H]^{+4}$), **HRMS** (ESI): Calculated for $C_{129}H_{218}N_{39}O_{34}$: 952.5504; found: 952.5505 ($[M+3H]^{+3}$).

*Synthesis of Tm**P**$(Man_3)_2$*

Following the general protocol of the SPPS for synthesizing a TAMRA labelled peptide with two α-D-mannose trisaccharide, Tm**P**$(Man_3)_2$ was obtained after RP-HPLC purification [Agilent Eclipse XDB-C18, 9.4x250 mm, H_2O (0.1% TFA)/ CH_3CN (0.1% TFA) 95:5→5:95 (0→35 min)] with an overall yield of 11% (38 mgs) and 99% purity. R_t 7.73 min (Fig. S10) [RP-HPLC Agilent SB-C18 column, H_2O (0.1% TFA)/ CH_3CN (0.1% TFA) 95:5→5:95 (0→12 min)]. **^{1}H-NMR** (500 MHz, D_2O, δ): 8.21 (s, 1H), 8.03-7.87 (m, 1H), 7.72-7.58 (m, 1H), 7.44-7.35 (m, 1H), 7.23-7.12 (m, 2H), 7.04-6.95 (m, 2H), 6.95-6.86 (m, 2H), 6.83 (s, 2H), 5.07-4.93 (m, 2H), 4.86-4.70 (m,

4H), 4.51-4.40 (m, 4H), 4.33-4.09 (m, 13H), 4.07-3.34 (m, 62.5 Hz, 36H), 3.18 (s, 12H), 3.14-3.03 (m, 16H), 2.94-2.78 (m, 2H), 2.36-2.11 (m, 2H), 1.95-1.03 (m, 57H), 0.95-0.58 (m, 30H). **MS** (ESI, H_2O): 1244 (100, $[M+3H+2TFA]^{+3}$), 1207 (78, $[M+3H+TFA]^{+3}$), 1169 (10, $[M+3H]^{+3}$), 905 (55, $[M+4H+TFA]^{+4}$), 604 (47, $[M+6H+TFA]^{+6}$), **HRMS** (ESI): Calculated for $C_{153}H_{258}N_{39}O_{54}$: 1168.6208; found: 1168.6204 ($[M+3H]^{+3}$).

*Synthesis of Tm**P**(Acetone)$_2$*

Following the general protocol of the SPPS for synthesizing a TAMRA labelled peptide capped with acetone, Tm**P**(Acetone)$_2$ was obtained after RP-HPLC purification [Agilent Eclipse XDB-C18, 9.4x250 mm, H_2O (0.1% TFA)/ CH_3CN (0.1% TFA) 95:5→5:95 (0→35 min)] with an overall yield of 12% (30 mgs) and 99.9% purity. R_t 8.21 min (Fig. S11) [RP-HPLC Agilent SB-C18 column, H_2O (0.1% TFA)/ CH_3CN (0.1% TFA) 95:5→5:95 (0→12 min)]. **^{1}H-NMR** (500 MHz, D_2O, δ): 8.07-7.89 (m, 2H), 7.55 (s, 1H), 7.03 (d, *J* = 9.2 Hz, 2H), 6.89-6.69 (m, 4H), 4.34 (d, *J* = 7.9 Hz, 4H), 4.27-3.93 (m, 13H), 3.40-3.22 (m, 2H), 3.10 (s, 12H), 3.07-2.98 (m, 16H), 2.31-2.11 (m, 2H), 1.89-1.63 (m, 12H), 1.60-1.10 (m, 57H), 0.88-0.64 (m, 30H). **MS** (ESI, H_2O): 1492 (8, $[M+2H+4TFA]^{2+}$), 1434 (10, $[M+2H+3TFA]^{2+}$), 1376 (8, $[M+2H+2TFA]^{2+}$), 918 (100, $[M+3H+2TFA]^{3+}$), 881 (100, $[M+3H+TFA]^{3+}$), 690 (18, $[M+4H+2TFA]^{4+}$), 662 (40, $[M+4H+TFA]^{4+}$), 632 (18, $[M+4H]^{4+}$). **HRMS** (ESI): Calculated for $C_{119}H_{201}N_{39}O_{22}$: 1264.2899; found: 1264.2902 ($[M+2H]^{2+}$).

General procedure for circular dichroism

Circular dichroism measurements were carried out using the following settings: acquisition range: 300-190 nm; band width: 1.0 nm; accumulation: 3 scans; data pitch: 1 nm; CD scale: 200 mdeg/1.0 dOD; D.I.T. (Data Integration Time): 1s; scanning mode: continuous; scanning speed: 200 nm/min. Measurements were done from 10°C to 60°C (data interval: 10°C; temp. gradient: 5°C /min) in a quartz cell of 0.2 cm path length at a final volume of 0.5 mL (HKR buffer or TFE) with a final peptide concentration of 200 μM.

The results are expressed as the mean residue molar ellipticity $[\theta]_{MRt}$ with units of degrees·cm^2·dmol^{-1} and calculated using the equation S1:

$$[\theta]_{MRt} = \frac{100 \cdot \theta}{C \cdot l \cdot N^o of\ residues} \qquad (S1)$$

where θ is the ellipticity (deg), C is the peptide concentration (M) and l is the cell path length (cm).[5,6]

NMR measurements

NMR experiments were acquired with 1.5 mM peptide samples prepared in phosphate buffer 20 mM containing 30% of deuterated trifluoroethanol (TFE-d_2) and 10 % of D_2O. 2D-TOCSY and 2D-NOESY spectra were acquired on a Bruker 500 MHz spectrometer at 298 K, with mixing times of 75 ms and 500 ms, respectively. Both experiments were recorded with 4096 data points in F2 and 256 data points in F1.

Peptide assignment were carried out by using CARA software[7] and structure calculations were performed by using CYANA 3.0 with distance restraints derived from the experimental NOEs.[8]

Cells lines and culture

Cell lines were incubated at 37°C, 5% CO_2, 95% humidity in an INCO 108 incubator (Memmert) with Dulbecco's Modified Eagle's Medium (4500 mg/L glucose, L-glutamine, sodium pyruvate

and sodium bicarbonate; Sigma-Aldrich), supplemented with 10% fetal bovine serum (Sigma-Aldrich) and 1% of Penicillin-Streptomycin-Glutamine Mix (Fisher). Each cell line was grown on four chamber glass bottom dishes and washed with HEPES–Krebs–Ringer (HKR) buffer (5mM HEPES, 137 mM NaCl, 2.68 mM KCl, 2.05 mM $MgCl_2$, 1.8 mM $CaCl_2$, pH 7.4) and nuclei were stained by incubation with 1µM Hoechst 33342 in HKR for 30 min. The peptide was diluted in HKR, DMEM or DMEM/FBS (10%) to obtain the different concentrations that were recalibrated by UV. Cells were incubated with the peptide for 30 min and then washed to remove excess peptide using an heparin solution (2x500 µL, 0.1 mg/ml) and HKR buffer (2x500 µL) before performing epifluorescence microscopy using a Nikon Eclipse Ti-E inverted microscope or confocal microscopy with a Leica SP5 microscope. Images were analyzed with ImageJ.

Cell viability: MTT assay

Cell viability was established by a standard MTT assay (Fig. S5). One day before the assay, a suspension of HeLa cells was plated in 96-well tissue culture plates (Costar 96 Flat Bottom Transparent Polystyrol) by adding 100 µL (150.000 cells/mL) per well. The next day, the medium was aspirated and cells were incubated with different concentrations of peptide diluted in HKR (50 µL/well). After 1 hour of incubation at 37ºC, the medium was aspirated and cells were washed with HKR buffer (2x100 µL/well). Then fresh medium (DMEM) containing 10% FBS (100 µL) was added to the cells during 3h. Control cells 100% were permorfed with only cell culture medium (100 µL final medium) and control cell 0% with TRITON solution. The viability was measured by quantifying the cellular ability to reduce the water-soluble tetrazolium dye 3-(4,5-dimethyl-2-thiazolyl)-2,5-diphenyl tetrazolium bromide (MTT) to its insoluble formazan salt as follows. MTT (5 mg/mL in PBS, 10 µL/well) was added to the wells and the cells were further incubated for 4 h. The supernatant was carefully removed and the water-insoluble formazan salt was dissolved in DMSO (100 µL/well). The absorbance was measured at 570 nm using a microplate reader (Infinite F200pro, Tecan). Data points were collected in triplicate and expressed as normalized values for untreated control cells (100% and 0%).

General protocol for flow cytometry

One day before the assay, different cell lines were plated in 96-well tissue culture plates (Costar 96 Flat Bottom Transparent Polystyrol) by adding 100 µL (150.000 cells/mL) per well. The next day, the medium was aspirated and cells were incubated with different concentrations of peptide (50 µL/well) in HKR buffer. After 30 min of incubation at 37ºC, the buffer was aspirated; cells were washed with heparin solution (1x100 µL, 0.1 mg/mL) and HKR buffer (2x100 µL). Finally trypsin 50 µL was added in each well and cells were incubated for 15 min at 37ºC. After this, 150 µL of a solution of 2% FBS and 5 mM EDTA in PBS were added to the cells. Cells were analyzed in a Guava EasyCyte (Millipore) cytometer and the results were processed in an InCyte software (GuavaSoft 3.2 Millipore).

Zebrafish experiments

One-year-old adult zebrafish (Danio rerio) were maintained in 30 L aquaria at a rate of 1 fish per liter of water on a recirculating system, in a controlled environment of 14-h light/10-h dark cycle at 28 ºC. Zebrafish embryos were obtained by massive spawning from breeding stocks of adult zebrafish.

48 hours post-fertilization (hpf) zebrafish embryos were exposed to 1 µM concentration of glycopeptides (namely Tm**P**$(Gal)_2$ and Tm**P**$(Man_3)_2$) in order to evaluate their uptake capacity into the embryo and, if possible, their biodistribution. This was possible because of fluorescence characteristics of glycopeptides analysed and transparency of fish embryos. Exposition took

place for 96 h, being fishes checked every 24 h. Pictures were taken with a Nikon AZ100 Zoom fluorescence microscope and analyzed with NIS Elements software (Nikon).

The protocols used in this study were performed in compliance with the EU animal experimentation regulation (EU, 2010) and were approved by the Bioethics Committee for Animal Experimentation CEEA-LU (Universidade de Santiago de Compostela, Spain). When needed, embryos were euthanized by tricaine (MS-222) overdose

Supporting figures for characterization

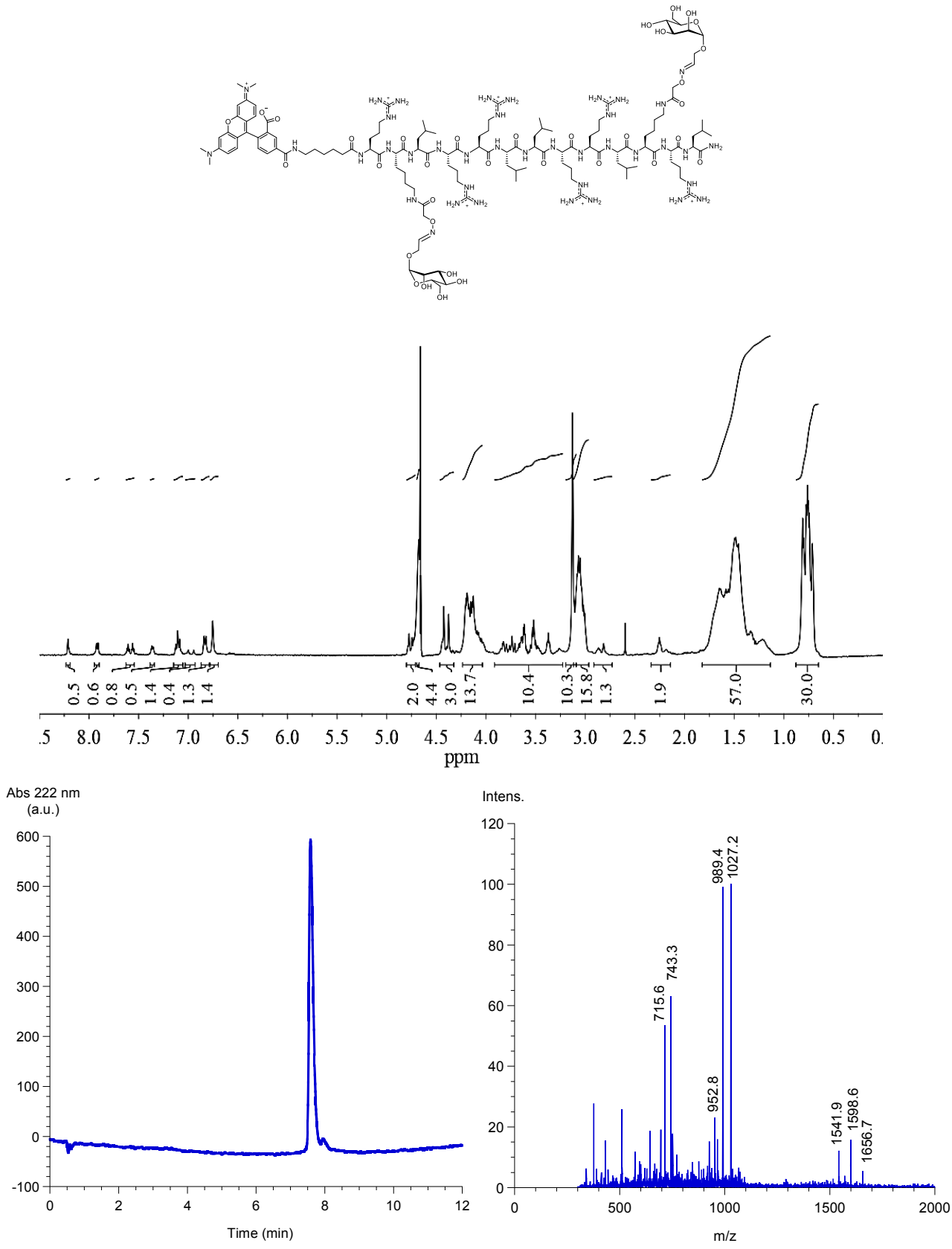

Figure S9. A) ^{1}H-NMR spectra in D_2O of Tm**P**$(Man)_2$. B) RP-HPLC-C18 column, H_2O (0.1% TFA)/ CH_3CN (0.1% TFA) 95:5→5:95 (0→12 min)]. (R_t 7.62 min) and ESI-MS of Tm**P**$(Man)_2$.

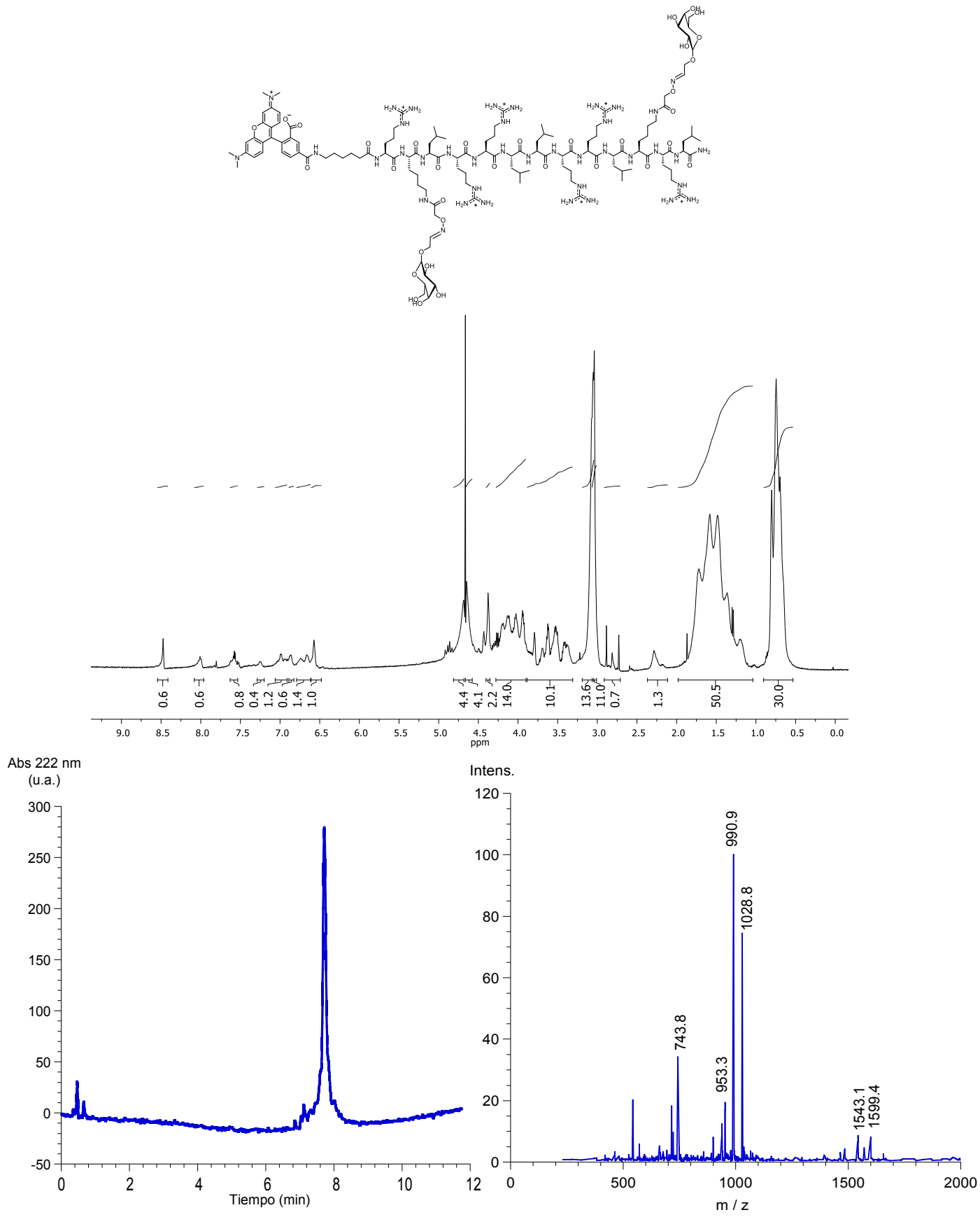

Figure S10. A) ^{1}H-NMR spectra in D_2O of Tm**P**$(Gal)_2$. B) RP-HPLC-C18 column, H_2O (0.1% TFA)/ CH_3CN (0.1% TFA) 95:5→5:95 (0→12 min)]. (R_t 7.81 min) and ESI-MS of Tm**P**$(Gal)_2$.

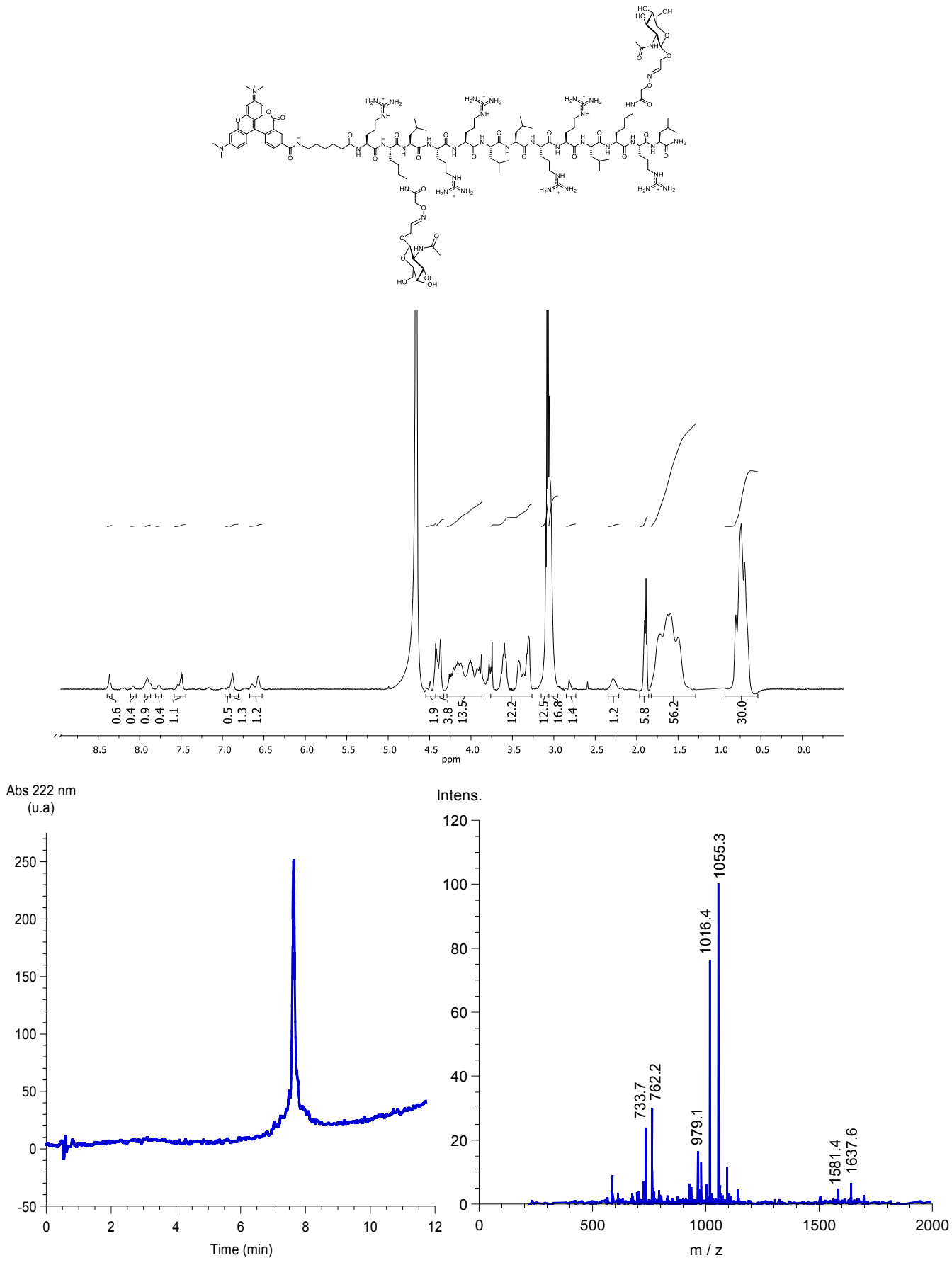

Figure S11. A) ^{1}H-NMR spectra in D_2O of Tm**P**$(NAG)_2$. B) RP-HPLC-C18 column, H_2O (0.1% TFA)/ CH_3CN (0.1% TFA) 95:5→5:95 (0→12 min)]. (R_t 9.90 min) and ESI-MS of Tm**P**$(NAG)_2$.

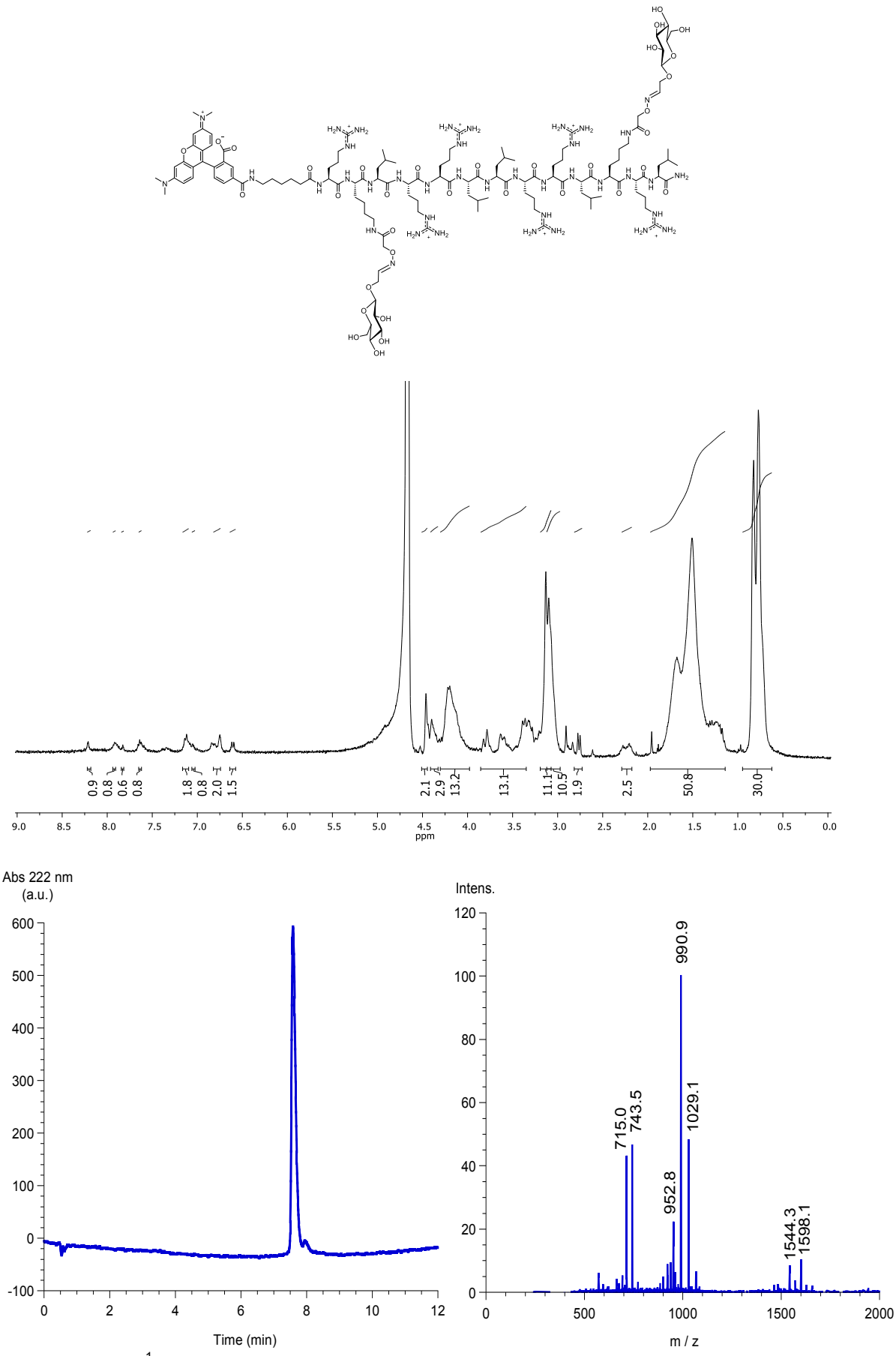

Figure S12. A) ^{1}H-NMR spectra in D_2O of Tm**P**$(Glu)_2$. B) RP-HPLC-C18 column, H_2O (0.1% TFA)/ CH_3CN (0.1% TFA) 95:5→5:95 (0→12 min)]. (R_t 7.59 min) and ESI-MS of Tm**P**$(Glu)_2$.

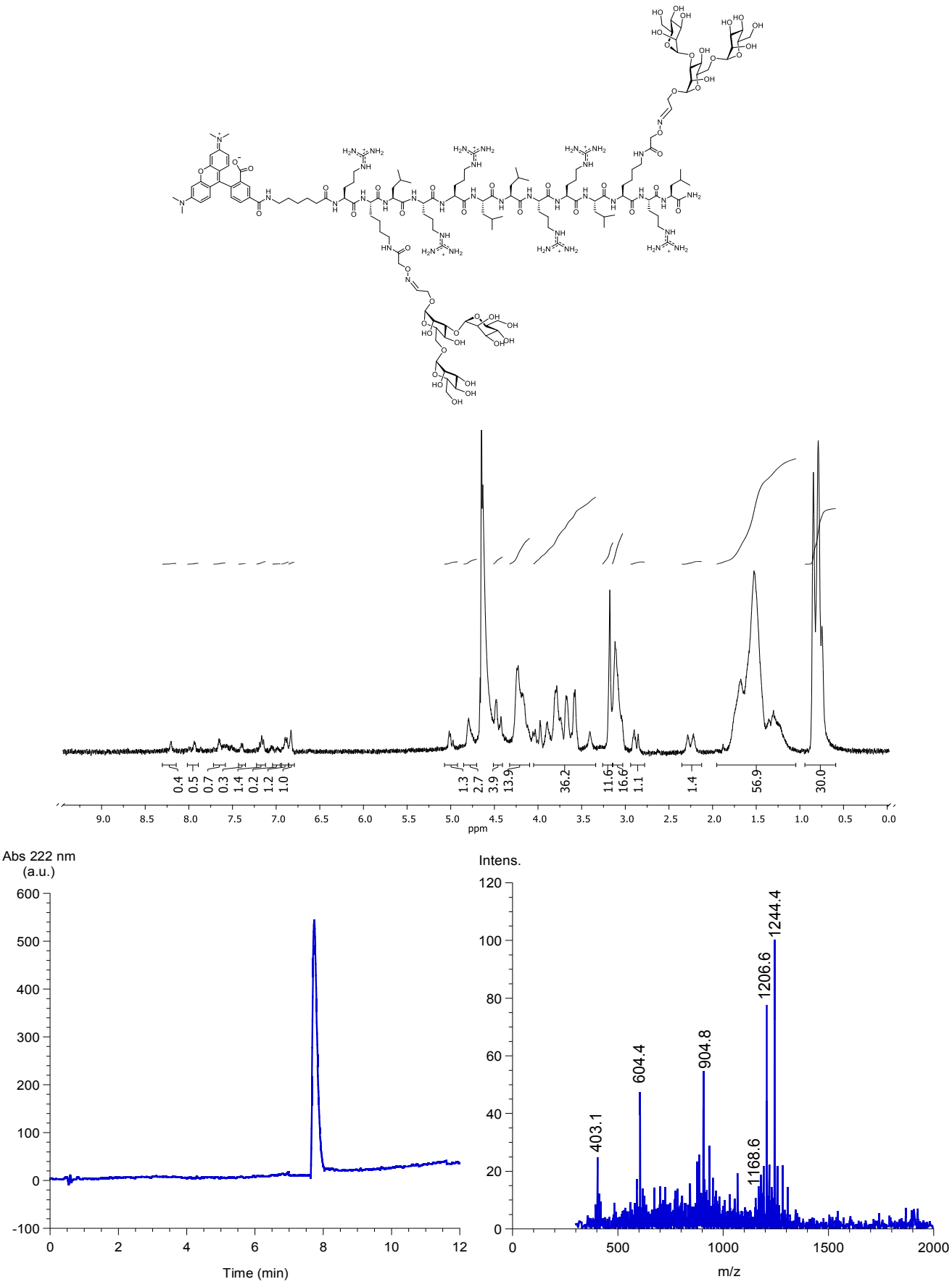

Figure S13. A) ^{1}H-NMR spectra in D_2O of Tm**P**$(Man_3)_2$. B) RP-HPLC-C18 column, H_2O (0.1% TFA)/ CH_3CN (0.1% TFA) 95:5→5:95 (0→12 min)]. (R_t 7.73 min) and ESI-MS of Tm**P**$(Man_3)_2$.

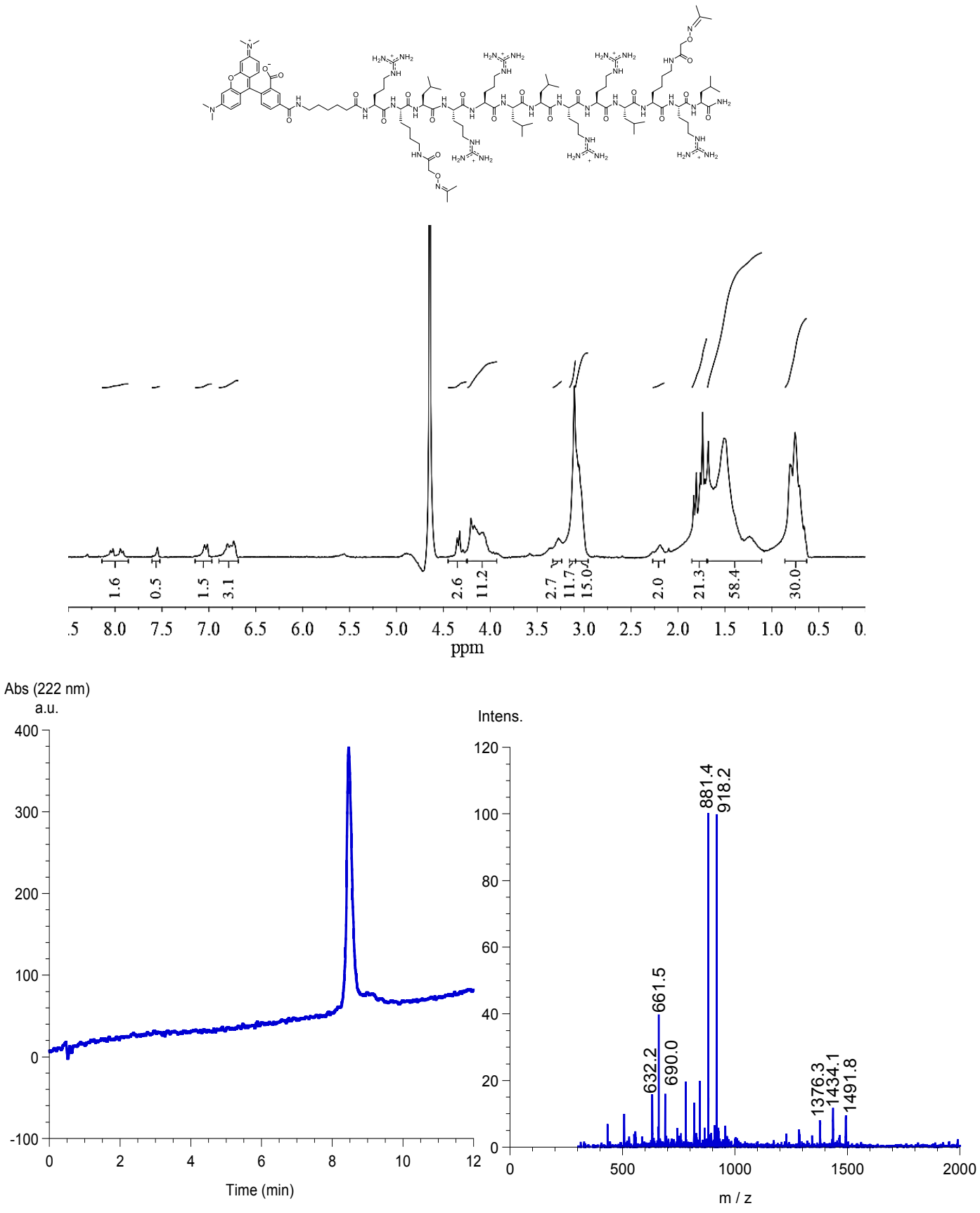

Figure S14. A) ^{1}H-NMR spectra in D_2O of Tm**P**(Acetone)$_2$. B) RP-HPLC-C18 column, H_2O (0.1% TFA)/ CH_3CN (0.1% TFA) 95:5→5:95 (0→12 min)]. (R_t 8.21 min) and ESI-MS of Tm**P**(Acetone)$_2$.

Supporting references

[1] R. Behrendt, P. White, J. Offer, *J. Pept. Sci.* **2016**, *22*, 4–27.
[2] M. Juanes, I. Lostalé-Seijo, J. R. Granja, J. Montenegro, *Chem. - A Eur. J.* **2018**, *24*, 10689–10698.
[3] C. K. O. E. Lorthioir, N. J. Parr, M. Congreve, S. C. Mckeown, J. J. Scicinski, S. V Ley, **2001**, *13*.
[4] J. Reina, A. Rioboo, J. Montenegro, *Synthesis (Stuttg).* **2018**, *50*, 831–845.
[5] S. Y. M. Lau, A. K. Taneja, R. S. Hodges, *J. Biol. Chem.* **1984**, *259*, 13253–13261.
[6] N. E. Zhou, C. M. Kay, R. S. Hodges, *J. Biol. Chem.* **1992**, *267*, 2664–2670.
[7] R. L. J. Keller, *The Computer Aided Resonance Assignment Tutorial*, **n.d.**
[8] P. Güntert, in *Meth. Mol. Biol.*, Humana Press, New Jersey, **n.d.**, pp. 353–378.

Entry for the Table of Contents (Please choose one layout)

Layout 1:

FULL PAPER

Text for Table of Contents

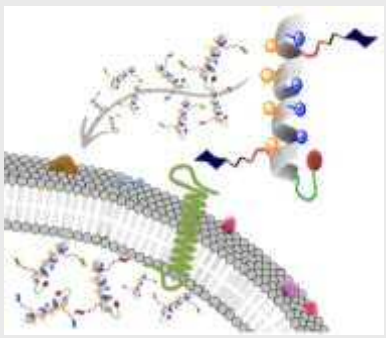

*Author(s), Corresponding Author(s)**

Page No. – Page No.

Title

Layout 2:

FULL PAPER

((Insert TOC Graphic here; max. width: 11.5 cm; max. height: 2.5 cm))

*Author(s), Corresponding Author(s)**

Page No. – Page No.

Title

Text for Table of Contents